CONF-9009267--4

PNL-SA-18535

PNL-SA--18535

DE91 004811

ATOMIC AND MOLECULAR PHYSICS IN THE GAS PHASE

L. H. Toburen

September 1990

Prepared for
DOE Conference on
Molecular and Biological
Effects of Radiation,
Woods Hole, MA
September 4-7, 1990

Work supported by the Office of
Health and Environmental Research
(OHER), U.S. Department of Energy
under Contract DE-AC06-76RLO 1830

Pacific Northwest Laboratory
Richland, Washington 99352

ATOMIC AND MOLECULAR PHYSICS IN THE GAS PHASE

L. H. Toburen
Pacific Northwest Laboratory
Richland, Washington 99356

Abstract

The spatial and temporal distributions of energy deposition by high-linear-energy-transfer radiation play an important role in the subsequent chemical and biological processes leading to radiation damage. Because the spatial structures of energy deposition events are of the same dimensions as molecular structures in the mammalian cell, direct measurements of energy depositions distributions appropriate to radiation biology are infeasible. This has lead to the development of models of energy transport based on a knowledge of atomic and molecular interactions process that enable one to simulate energy transfer on an atomic scale. Such models require a detailed understanding of the interactions of ions and electrons with biologically relevant material. During the past 20 years there has been a great deal of progress in our understanding of these interactions; much of it coming from studies in the gas phase. These studies provide information on the systematics of interaction cross sections leading to a knowledge of the regions of energy deposition where molecular and phase effects are important and that guide developments in appropriate theory. In this report studies of the doubly differential cross sections, crucial to the development of stochastic energy deposition calculations and track structure simulation, will be reviewed. Areas of understanding are discussed and directions for future work addressed. Particular attention is given to experimental and theoretical findings that

have changed the traditional view of secondary electron production for charged particle interactions with atomic and molecular targets.

Introduction

The importance of the spatial and temporal distributions of ionization in determining the subsequent chemical and biological damage induced by ionizing radiation has long been recognized (see, for example, Lea, 1947). During the past 25 years we have seen a continuing evolution in the need for understanding the details of these distributions in increasingly smaller volumes in order to interpret results obtained in studies of radiation biology. This need spawned the field of microdosimetry and has lead to the development of computational tools in charged-particle track simulation to investigate energy deposition in volumes smaller than can be reached by experimental microdosimetric techniques. Computational techniques also provide flexibility to incorporate target heterogeneity and phase important to biological media.

For high-linear-energy-transfer (high-LET) radiation the traditional concept of dose, that of average energy imparted per unit mass, is inappropriate owing to the highly localized nature of the energy deposition. For a dose of a few rads delivered by alpha particles, for example, only about 1 cell in 10 may be traversed by an alpha particle and the cells that do get hit may receive 10 times the average dose estimate. Thus, assessing the biological effects from alpha particles, or other high-LET radiation requires a knowledge of the energy deposition, or dose, at the microscopic level. Studies of DNA strand

breaks induced by ^{125}I, for example, indicate that an energy of 17.5 eV deposited in the sugar-phosphate is adequate to cause a DNA strand break (Charlton, 1988). These estimates are made by comparing energy deposition distributions determined from track simulation calculations with measurements of the frequency of strand breaks in cells irradiated with known amounts of ^{125}I incorporated into the cellular DNA. An experimental measurement of the energy deposited in volumes this small is, of course, infeasible, thus one must rely on accurate models of energy deposition and transport to make such comparisons.

A description of the interaction of high-LET radiation with cellular DNA requires a knowledge of both the structure of the particle track and the DNA target structure. An example of the relative size of the structural features of a 2-MeV alpha particle track and representative target structures of a DNA molecule are shown in Fig. 1. This illustration was prepared by Walt Wilson in our laboratory using the Monte Carlo track structure code MOCA15 that he has developed in collaboration with Herwig Paretzke (Paretzke, 1987). This code scores both excitations and ionizations for interactions of charged particles in a water vapor medium. For this example secondary electrons were followed until degraded in energy to 25 eV, where they are considered locally absorbed. The example given in Fig. 1 illustrates several features that can be derived from stochastic, atom-by-atom, descriptions of a charged particle track. First, the structures of the track resulting from energy transport by delta-rays are of the same order-of-magnitude in size as the nucleosome structures of DNA. One may expect multiple sites of damage in the DNA if one of these track features should correspond in space to that of the nucleosome.

The example also illustrates the effect of inner-shell ionization of the oxygen atom of the constituent water vapor molecule. The energetic delta-ray shown moving up through the nucleosome in Fig. 1A is the result of the ejection of an electron from the K-shell of oxygen; the second electron emanating from that point is the Auger electron following relaxation of the inner-shell vacancy.

The end-on view of the track in fig. 1B illustrates what some authors have described as the "core" and the "penumbra" regions of charged particle tracks. It can be shown, however, that in this case this effect is simply the result of the projection displayed and has little physical meaning. To illustrate this we have expanded the scale in Fig. 1C to look at the individual energy deposition events on the same scale as the atomic positions of the DNA molecule. Note that on this scale there is no evidence of a track core. Certainly it is possible that ionizations may occur on adjacent atoms, but the probability for this occurring is low for even a particle with LET this high (approximately 165 keV/micrometer). It should also be noted that this illustration is a 2-dimensional projection of a 3-dimensional structure, thus individual ionizations/excitations are actually distributed further apart on the average than they appear in the figure.

It is obvious that a comprehensive knowledge of the interactions of charged particles with biological material must be known if one is to accurately reliably assess the spatial patterns of excitations and ionizations for charged particles in the heterogeneous environment of the biological cell. A detailed set of quantitative information is required for the production and

subsequent slowing down of secondary electrons ejected in ionizing collisions between the moving ion and the atomic and molecular constituents of the media. Such information must be in the form of absolute cross sections and must incorporate knowledge of the atomic, molecular, and phase of the target. The full extent of the cross sections needed in track structure simulation depend on the intended application and the mechanism for subsequent chemical and biological damage assumed. Most applications of track structure simulation have involved the investigation of microdosimetric distributions of energy deposition by secondary electrons for different types of radiation of importance to the field of Radiation Dosimetry or have provided the initial pattern of energy deposition for investigation of the time sequence of chemical reactions that follow degradation of secondary electrons. Such calculations rely primarily on an accurate knowledge of the production and transport of secondary electrons that form the basic structure of charged particle tracks.

Knowledge of the physics of electron production and degradation has been the key to development of reliable stochastic track structure models. However there are other processes of energy deposition in the track of a charged particle that are less common, but may produce the unusual events that the biological system is incapable of handling. Such events as multiple ionizations of constituents of the DNA may produce irreparable molecular/biological damage, or the correlated electrons emitted in such interactions may induce subsequent chemical damage unique to the biological repair system. Temporally and spatially correlated events may also be stimulated by inner-shell ionization or by simultaneous electron loss and

target ionization involving projectiles that carry bound electrons, such as He^+ ions formed in the slowing down of alpha particles. Many of these processes are only beginning to be understood from a physical point of view and have yet to be investigated as to their biological implications.
The principal source of data needed as input for calculations that simulate the stochastic processes that form charged particle tracks, such as those shown in Fig. 1, are the cross sections for the production and transport of secondary electrons. These cross sections must be absolute in magnitude and differential in ejected electron energy and emission angle. The considerable progress in measurements of these cross sections and in our ability to model their systematics during the past 20 years has been key to performing reliable track structure simulations. Prior to these advances homogeneous track structure models (Butts and Katz, 1967; Chatterjee and Shaefer, 1976) were based on the early collision physics theory of Bohr (Bohr, 1947). In those models the probability of ionization was obtained from the free electron Rutherford cross section, electrons were assumed to be emitted perpendicular to the particle path, and straight line trajectories were assumed in order to calculate electron ranges. In addition, Chatterjee and Shaefer assumed that half the energy lost in collisions between the incident particle and constituents of the medium went into excitation, thus contributing to a high energy density in the core of the particle track. As we shall see many of these assumptions have proven to be inaccurate as experimental data have become available to test our understanding.

In this paper we look briefly at the extent of our knowledge of differential ionization cross sections for energy loss by charged particles. As Inokuti

has stated, to be useful cross sections must be "right, absolute, and comprehensive" (Inokuti, 1989). In this review, these virtues of the experimental data are addressed. The discussion is organized by incident particle; that is, we start by discussing electron impact, than proton impact, followed by heavier ion impact. The final section looks briefly at the relative importance of other processes, such as charge transfer and multiple ionization. Although an effort is made to be comprehensive in this review, the field is sufficiently large that pertinent data is surely to have been inadvertently left out. We apologize to those investigators, and to the reader, for those emissions.

Doubly-Differential Ionization Cross Sections

Electron Impact

The primary components of any track structure simulation are the production and slowing down of secondary electrons. Therefore it is important that one has a detailed knowledge of the interaction cross sections for electrons with the stopping media of interest. A recent review by Paretzke (1987) provides an excellent guide to the literature of electron interactions of interest to radiobiology and to radiation chemistry. Table I, in the appendix of this report, provides a listing of the measured doubly-differential electron emission cross sections, differential with respect to "ejected" electron energy and emission angle, obtained from a search of the literature. Since electrons are indistinguishable the slower of the two electrons leaving a collision is defined as the secondary electron. To completely define the

collision for electron impact one would need to measure triply-differential cross section, ie., also detect the scattering angle of the primary electron. A limited number of triply-differential cross sections have been measured for simple gas targets such as helium and argon (see, for example Beaty, et al (1978); and Hong and Beaty, (1978)), however such data have been of little practical use in track structure calculations and are considered out of the scope of the present review.

Although Table I illustrates that there are a relatively large amount of data available on the doubly-differential cross sections for ionization by incident electrons only a limited subset of this data is directly appropriate to targets of interest to radiological physics. In addition, where data have been obtained by different groups, such as the cross sections for ionization of water vapor shown in Fig. 2, there is considerable scatter in the data for different investigators. In general the agreement between the data of Bolorizadeh and Rudd (1986), Opal et al. (1971), and Oda (1975) is quite good for intermediate angles. However, at both, large and small emission angles, the cross sections of Opal et al. tend to be smaller than the other two measurements. These differences result from different methods of accounting for the finite size of the target as one views it from different angles. The true cross sections are probably somewhere between the extremes represented by the data of Bolorizadeh and Rudd and Opal et al.

Because of the scatter in experimental data from different sources a good deal of effort has gone into theoretical techniques to evaluate the accuracy of measured cross sections. Following the lead of Platzman, Kim has explored the

consistency of experimental data for electron and proton collisions using well established theory (Kim, 1972, 1975, 1975a; Kim and Inokuti, 1973; Kim and Noguchi, 1975). The Mott cross section is used to test the behavior of fast electrons ejected by fast primary electrons, whereas the slow electrons are analyzed in terms of the dipole oscillator strengths as prescribed by the Born approximation. An example of the utility of this method is shown in Fig. 3 taken from Kim (1975), where the ratios of the experimental cross sections to the corresponding Rutherford cross sections are plotted as a function of the reciprocal of the energy loss. Plotted in this way the area under the curve is proportional to the total ionization cross section and the shape of the low-energy portion of the curve is representative of the dipole oscillator strength. The fraction of the electrons ejected with energies between the shaded vertical lines between w=o and 15.6 eV represents those electrons that are unable to produce further ionization as they slow down in the target medium. In the example shown in Fig.3, the only experimental data used to establish the family of curves were single-differential cross sections for electron emission by 500-eV incident electrons. Those data were used, along with the dipole oscillator strengths, to define the overall shape of the curve for 500-eV primaries. The magnitude of the cross sections was then established by normalization of the area under the curve to the total ionization cross section. Curves for other primary energies could then be drawn by extrapolation based on maintaining 1) a curve shape consistent with the optical oscillator strengths, 2) the proper integrated area consistent with total ionization cross sections, and 3) the proper kinematic limit to the secondary electron energy consistent with the maximum energy transfer. Models of this type provide means to evaluate experimental consistency, to

extrapolate data to regions where data are unavailable, and provide convenient methods of introducing data into computer codes for track structure calculations. This technique of data analysis and extrapolation takes advantage of the availability of a wide range of experimental data on total ionization cross sections (see, for example, reviews by Schram et al.,1965, and Shimamura, 1989) and oscillator strengths (Berkowitz,1979). In addition, the use of spectra based on oscillator strength distributions has the potential for application to both gas and condensed phase targets by simply using the proper oscillator strengths. These techniques will be described in more detail in the following sections with regard to their application to proton-induced ionization. For greater detail in the application of this method to electron-impact ionization the interested reader is directed to the work of Kim referenced above, as well as to the review of Paretzke (1987), and to studies by Miller and Manson (1984), and Miller et al. (1987).

One of the large gaps in our knowledge of interactions of electrons with biologically relevant material is the lack of direct measurements of these processes in the condensed phase. Presently the basis of condensed phase electron transport used in track structure simulation is deduced from the theory of charged particle interactions in condensed phase, and from oscillator strengths for photoabsorption (Berkowitz, 1979). During the past few years, however, there have been significant advances in our understanding of electron interactions in the condensed phase brought about by the pioneering work of Leon Sanche and his coworkers (Michaud and Sanche, 1987; Sanche, 1989; Cloutier and Sanche, 1989; Marsolais and Sanche). Measurements that they have conducted on the scattering of low-energy electrons in thin

films have provided detailed information on the energy loss mechanisms associated with the slowing down of slow electrons. A particularly interesting feature in the preliminary studies has been the similarity of elastic and inelastic electron scattering processes in the solid to those observed in the gas phase, eg., resonant processes, such as transient negative-ion formation (Sanche, 1989), are strong feature in the energy-loss spectra for very low-energy electrons.

Proton Impact

There has been a wide range of experimental and theoretical studies of doubly-differential cross sections for proton impact ionization of atomic and molecular targets. Much of this work was funded by the Radiological and Chemical Physics Program of the Department of Energy and was directed toward understanding the effects of molecular structure and to developing models applicable to track structure calculations. Reviews of doubly-differential cross sections have been published by Toburen (1982, 1979) and by Rudd (1975). An updated listing, first published by Toburen (1982), of the doubly-differential cross sections available for proton impact is presented as Table II in the appendix. This list focuses on studies that report absolute cross sections and those that provide a broad spectrum of energies and angles. Table does not include studies of "convoy electrons" (see, for example, Breinig, et al., 1982) or studies that focus on a narrow angular range, eg. electrons ejected at zero degrees; such studies are not considered highly relevant to Radiological Physics and would require a full review on their own. From Table II we see that data are available that span the regions of low (5-

50 keV), intermediate (50-300 keV), and high (greater than about 300 keV) proton energies; these energy ranges reflect regions requiring different theoretical approaches. Only a few molecules, eg., hydrogen, nitrogen, oxygen, and water vapor, have been studied through all the energy ranges. Those molecules, however, provide a good representation of the constituents of tissue. The majority of the data base for investigating molecular effects has been developed in the region of high-energy protons.

An indication of the precision of the various measurements can be addressed by an evaluation of the uncertainties contributing to the individual measurements and by comparison of measurements of different investigators where they overlap. A comparison of doubly-differential cross sections for ejection of electrons from nitrogen by 0.3 Mev protons measured by three different research groups is shown in Fig. 4. For ejected electron energies greater than about 15 eV the agreement is well within the stated 20% uncertainties in the individual measurements. For lower energy ejected electrons the data diverge due to the effects of stray electrostatic and magnetic fields on the transmission of the electrostatic energy analyzers used in the cross section measurements. To resolve the uncertainties at low energies a time-of-flight (TOF) technique was developed that could measure relative cross sections for ejected electron energies in the range from 1 to 200 eV (Toburen and Wilson, 1975). The solid lines in Fig. 4 were derived from TOF measurements normalized to the electrostatic results at 100 eV. This combination of electrostatic and TOF measurements provide reliable cross sections for the ejected energy range from 1 to 5000 eV, thus providing a wide range of data for analysis of cross sections systematics and for development of theoretical

models.

To test the "correctness", as defined by Inokuti (1989), of the measured cross sections we can make use of simple theoretical arguments for the asymptotic behavior of cross sections as has been advocated by Kim and Inokuti (1973). For example, the Rutherford formula given as

$$\frac{d\sigma}{dE} = \frac{4\pi a_0^2 z^2}{T} \frac{R^2}{E^2} \qquad (1)$$

where a_0 is the Bohr radius, Z is the projectile charge, R is the Rydberg energy, $T=mv^2/2$ (m is the electron mass), and $E=\epsilon+I$ (ϵ is the ejected electron energy and I the ionization potential), should provide an accurate estimate of the cross section when the energy loss is large compared to the binding energy of the ejected electron, but smaller than the kinematic limit of energy transfer in a binary collision. Thus if we plot the ratio of the measured cross section to the Rutherford cross section the ratio should approach a constant value for high energies of the ejected electron and, since the Rutherford formula gives the cross section per target electron, the magnitude of that constant should be equal to the number of electrons in the atomic or molecular target. In Fig. 5, this ratio, Y(E,T), is plotted versus E for an atomic helium target. In this illustration the ratios approach a value of approximately 2.2 which is indicative that the measured cross sections may be systematically 10% too large. Similar ratios are plotted in Fig. 6 for a wider range of proton energies and an atomic neon target. In principal, for an atom such as neon, where the electron can be ejected from inner shells or sub-shells, the ionization potential used in the Rutherford formula should reflect the origin of the electron. However, the experiments are not able to

determine the origin of the detected electron, therefore, the ratio is calculation assuming that all electrons originate from the valance shell (Toburen et al.,1978). For neon the ratio Y(E,T) approaches a value of approximately 10, indicative of the number of bound electrons in the atom; the peak observed at approximately 800 eV results from Auger electron emission following K-shell vacancy production. For the highest energy protons Y(E,T) approaches a value somewhat greater than 10, the total number of electrons in neon, again indicative that the experimental values may be systematically about 10% higher than would be expected. It should be noted, however, that the ratio for 1.5 MeV protons reaches a plateau at approximately 8 which is in good agreement with the Rutherford prediction if only the outer shell electrons participate; the inner-shell electrons are tightly bound and contribute little to the Rutherford cross section at this proton energy. An increased scatter in the data is observed for the higher energy ejected electrons shown in Fig. 6. This scatter occurs because the cross sections are becoming significantly smaller and statistical uncertainties are greater; the $1/E^2$ factor in the Rutherford cross section masks the absolute value of these cross sections. The Rutherford analysis generally confirms that the differential cross sections obtained in our work at the Pacific Northwest Laboratory (PNL) are accurate to within the stated 20% absolute uncertainties derived from the experimental parameters; data from other laboratories are generally at lower proton energies and not amenable to this theoretical test, but where data from different laboratories overlap there is good agreement.

Data have been obtained for a wide range of molecular targets for investigating the effects of molecular structure on electron emission cross

sections . In Fig. 7 are displayed the single differential electron emission cross sections for a number of carbon containing molecules plotted as the ratio to the respective Rutherford cross sections. The horizonal lines with the number to the right each give the Rutherford estimate of the asymptotic value those cross sections should attain. This agreement between experimental data and the predictions is simply a confirmation of the Bragg rule for scaling cross sections for emission of fast electrons, or a statement of the independent particle model for ionization. One must be careful at this point to stress that this is a scaling feature of collisions involving large energy loss and it does not apply to soft collisions; this will be discussed in detail later. It does, however, provide justification for application of simplified theory and scaling techniques that are very useful in track structure calculations.

The limits of applicability and reliability of various theoretical calculations can be assessed by comparison of their predictions to experimental data. In Fig. 8 the results of binary encounter theory, the Born approximation, and Rutherford theory are plotted as the ratio to the corresponding Rutherford cross section for ionization of the outermost shell of neon. The primary reason for comparing results by dividing by the Rutherford cross section is that the principal dependence on energy loss, $1/E^2$, is removed and one can compare data on a linear, rather than a logarithmic scale, thus accentuating spectral features. The gradual increase in the plotted Rutherford cross section plotted in this way occurs because it was calculated including electrons from all shells of neon, with their respective binding energies (Kim, 1975), and at larger values of the energy

loss the more tightly bound electrons contribute more to the total; the Rutherford cross section in the denominator of the calculated ratio is taken as the valance shell cross section as discussed above.

For a 1 MeV proton interacting with a free electron the Rutherford theory would predict an abrupt decrease in the cross section at approximately 160 Ry as that is the kinematic maximum in the energy that can be transferred in the classical proton-electron collision. The measured cross sections show a gradual decrease in magnitude between approximately 100 and 160 Ry reflecting the momentum distribution of the bound electrons. The increasing Rutherford cross section, owing to inner shell contributions, combined with the decrease in the experimental values near the maximum energy transfer, owing to binding effects, renders Rutherford theory inappropriate as a definitive test of the accuracy of measured cross sections in this proton energy range. At higher proton energies, as shown in Fig. 6, a plateau value of 10 can be expected over a broader ejected electron energy range.

Binary encounter theory (reviewed by Rudd, 1975) extends the classical Rutherford-like approach to collisions with electrons that are not at rest, includes effects of collisions with electrons that have an initial velocity distribution owing to the fact that they are bound to the atom. By integrating over a quantum mechanical distribution of bound electron velocities the high energy portion of the ejected electron spectra is well represented by this semi-classical approach. The only parameter that is not well defined in this computational technique is the mean of the initial distribution of kinetic energies exhibited by the orbital electrons.

Calculations that assume the initial kinetic energy is equal to the binding energy, BE_I, and that use the kinetic energy derived from Slater's rules (see Robinson, 1965), BE_S, are shown in Fig. 8; the use of Slater's rules seems to provide a slightly better agreement at high energies that the binding energy approach. For low-energy electron emission neither approach is very good, although the use of Slater's rules extends the agreement with experimental data to somewhat lower energies.

The results of calculations based on the plane wave Born approximation (Toburen et al., 1978) are also shown in Fig. 8. This calculation is in good agreement with the measured differential cross sections for ejection of low-energy electrons and with the independent measurement of Grission et al. (1972) for electrons ejected with zero kinetic energy; the calculation was not carried out to ejected electron energies greater than 64 Ry because it is based on a partial wave analysis and the number of partial waves necessary to describe the higher energy processes makes the calculation unwieldy. Similar calculations are in good agreement for helium targets (Manson, et al., 1975) The use of this technique for molecules has not been attempted, however, due to a lack of adequate wave functions to describe the molecular systems.

The data shown in Fig. 8 clearly illustrate the limitations of classical and semi-classical theory for predicting the cross sections for ejection of low-energy electrons. The relative importance of this region of the spectra, however, is illustrated in Fig. 9 where ejected electron distributions are displayed for ionization of several different molecules by 1 MeV protons. The hydrocarbons referenced in Fig. 9, are the same as those of Fig. 7, now scaled

on a per "effective" electron basis. Here the effective number of electrons in a molecule is taken as the total minus the K-shell electrons (Wilson and Toburen, 1975; Lynch et al., 1976) ; from the data for neon shown in Fig. 6 one would not expect the K-shell electrons to contribute significantly to the emission cross sections for ionization of first row elements by 1 MeV protons. Note the large differences in the electron yields associated with different molecules as the ejected electron energies decrease below approximately 20 eV. This is also the portion of the emission spectrum that is the major contributor to the total yield of electrons and therefore directly influences the total ionization cross section.

As was discussed above for electron impact, one can make use of the analysis developed by Kim to focus on the accuracy and consistency of the low-energy portion of the ejected electron spectra. As pointed out by Kim and Noguchi (1975), the area under the curve in a plot of Y(E,T) versus 1/E can easily be shown to be proportional to the total ionization cross section:

$$\sigma_{ion} = \int_{B}^{E_o} \frac{d\sigma}{dE}\, dE = \int_{1/E_o}^{1/B} \frac{d\sigma}{dE}\, E^2\, d\left(\frac{1}{E}\right) \qquad (2)$$

where B is the electron binding energy and E_o is the incident ion energy. Such a plot is useful for testing absolute normalization of the differential cross sections and for determining the importance of specific features of the spectra as contributors to the overall yield of ionization. Total ionization cross sections are available with accuracies of 5% to 10% for a wide range of atoms and molecules (Rudd et al., 1985).

The Bethe-Born expansion of the differential cross section provides a convenient framework to investigate the features of the single differential cross sections and their dependence of projectile parameters. The Bethe-Born formula can be written (Miller et al., 1987) as

$$\frac{d\sigma}{dE} = \frac{4\pi a_o^2 z^2}{T}\left[\frac{R^2}{E}\frac{df}{dE}\ln\left(\frac{4T}{R}\right) + B(E) + O\left(\frac{E}{T}\right)\right] \qquad (3)$$

where most symbols are defined as in eq. 1, above, and df/dE is the optical oscillator strength distribution. Expressed in this way B(E) includes contributions independent of T, and O(E/T) contains contributions of higher order in E/T. Because of the logarithmic dependence of the term involving the oscillator strength the spectra should become increasingly optical in nature as the ion energy increases. This is seen in Fig. 10, where data for ionization of helium by protons of different energies are shown; also shown are data for 500 eV electrons (Opal et al.,1971); these are of comparable velocity to the 1 MeV protons. The data displayed in Fig. 10 show the importance of knowing the shape of the low-energy portion of the spectra if one is to be able to gain an accurate knowledge of the total yield of electrons. For proton impact on a helium target a major fraction of the electrons have energies less than 25 eV (1/E=0.27). This presents no difficulties where cross section have been measured using both, electrostatic and TOF techniques, such as was done for the helium data in Fig. 10. However, where TOF is not available there may be large uncertainties in the low-energy portion of the spectra; see, for example the data in fig. 4. To overcome

these uncertainties Miller et al. (1983) applied the Bethe-Born approximation Kim and Inokuti (1973) to the analysis of proton impact data.

Inspection of eq. 3 indicates that if we have experimental data at any proton energy for which the Born approximation is valid those data can be used with optical oscillator strengths to evaluate what has been called the hard collision component of the interaction B(E); this assumes that terms of higher order in E/T are negligible. Since B(E) is independent of the incident proton energy, once determined that spectrum can be used to obtain cross sections at other energies. In practice experimental data are used to obtain B(E) for low-energy ejected electrons and the results are than merged with binary encounter theory to obtain an estimate of B(E)+0(E/T) for high ejected electron energies to give the full spectrum; binary encounter has been shown to describe fast ejected electrons quit well. The hard collisions contribution, B(E), found by Wilson et al. (1984), for ionization of water vapor by protons is shown in Fig. 11. Although B(E) is theoretically independent of ion energy there was considerable scatter among the data for B(E) derived from different proton energies. To determine the spectrum of B(E) from these data for use in calculating emission cross sections a simple average of the experimental values at different ion energies (the solid line in Fig. 11) was performed. Cross sections derived from this determination of B(E) are shown in Fig. 12. This model of the differential cross sections is in good agreement with the 0.5- and 1.5-MeV data as it must be, since these data were used in the determination of B(E); there is also good agreement with 3.0- and 4.2-MeV proton results obtained with a different experimental system and not included in the fitting process. An important asset of this technique

is the high degree of accuracy that can be obtained for the low-energy portion of the spectra owing to the use of optical oscillator strengths that dominate in this region.

Models of the ejected electron spectra based of eq. 3 rely on two primary sources of experimental data; differential electron emission cross sections for at least one ion energy and a source of optical oscillator strengths. We have discussed the electron spectra at length, but have said little regarding the availability of oscillator strengths. For the water vapor data discussed above, oscillator strengths were derived from the photo absorption cross sections compiled by Berkowitz (1979) using the expression

$$R \frac{df}{dE} = \frac{\sigma(Mb)}{8.07} \qquad (4)$$

where σ is the photo absorption cross section in units of megabarns and R=13.6, a good review of photoabsorption cross sections is also given in a technical report by McDaniel et al. (1979). Oscillator strengths are also available for a number of molecules of biological interest, such as DNA (Inagaki et al. (1974); Sontag and Weibezahn, 1975) and DNA bases (Fujii et al., 1986; Dillon, 1990). We can also expect considerable progress in the measurement of photoabsorption cross sections as synchrotron light sources become more widely used.

One of the shortcomings of models of secondary electron emission cross sections based on Bethe-Born theory, as expressed in eq. 3, is that the application is limited to ion energies that are sufficiently large for the

Born approximation to be valid. A model developed by Rudd (1988) overcomes this difficulty by incorporating aspects of molecular promotion theory to enable extensions of the model to low-energy ions. Rudd's model is not as versatile as the Bethe-Born, however, with respect to changing target parameters and it requires a much more extensive set of data to determine the full range of model parameters. Rudds model is based on the molecular promotion model at low energies and on the classical binary encounter approximation, modified to agree with Bethe-Born theory at higher energies. In total, Rudd's model requires 10 basic fitting parameters for each electronic shell of each target. These parameters have been published for proton impact ionization of H_2, He, and Ar (Rudd, 1988) and He, Ne, Ar, and Kr (Cheng et al., 1989). Model parameters for N_2, CO_2, H_2O, and O_2 are available from Rudd by private communication. An example of the results of Rudds model fit to molecular nitrogen data is shown in Fig. 13 for proton ionization of molecular nitrogen. This example illustrates the wide range in proton energy attainable by this model. The experimental data shown in Fig. 13 also illustrates the excellent agreement among the different experimental groups; Rudd (1979), Crooks and Rudd (1971), Toburen (1971), and Stolterfoht (1971). The arrows in the figure point to the electron energy where one would expect to see enhancement of the cross sections by the process of continuum-charge-transfer (CCT). This mechanism can be described as an electron being "dragged" out of the collision by the proton owing to the coulomb attraction, but failing to be captured into a bound state of the projectile (Rudd, 1975). This mechanism should enhance the cross section for electron energies where the velocity of the out-going electron and proton are comparable; the arrows in Fig. 13 are placed at those electron energies. The lack of observable

enhancement in the single differential cross sections at the appropriate energy is evidence that this mechanism does not contribute markedly to the total electron yield; the model does not include any theoretical mechanism for this process.

To this point the discussion has focused on singly differential cross sections for electron ejection. However, a crucial source of data for the determination of the spatial distributions of energy deposition around charged particle tracks is the angular distribution of ejected electrons. In Fig 13, angular distributions are shown for ejection of electrons of several energies from collisions of 2 MeV protons with a helium target. Also shown are the results of a binary encounter calculation of Bonsen and Vriens (1970) and those of a plane wave Born calculation of Madison (1973). This illustration emphasizes that the electrons are not, as previously assumed, ejected at 90 degrees to the proton path. There is a sizeable component of the cross section for electron ejection at both large and small angles. Also note that binary encounter theory underestimates the cross sections at large and small angles by as much as an order of magnitude. The use of the plane wave Born approximation improves the estimates at the large and small angles considerably, however there are still discrepancies at small angles for intermediate electron energies. These remaining discrepancies are the result of an enhancement of the cross sections by the process of continuum-charge-transfer (Rudd, 1975). This ionization mechanism, although not significant in the singly differential cross sections (see Fig. 13), plays a sizeable role in the doubly differential cross sections for small emission angles; it has not been included in the plane wave Born calculations shown in Fig. 14. The

theory of the continuum-charge-transfer (CCT) process was first carried out by Macek (1971). The results of Macek are compared in Fig 15 to Born results without CCT and to measurements from our laboratory for electrons ejected with velocities near that of the incident proton (the equivalent electron velocity for a 1 MeV proton is 544 eV) where the maximum contribution from CCT is expected. The calculation of Macek is shown to be in excellent agreement with the measurements. It should again be emphasized, that although the CCT contributions may enhance the doubly differential cross sections by as much as an order of magnitude in certain regions of the spectra, the contribution to the total yield of electrons in small.

For molecular targets, there is a great deal of similarity in the angular distributions of electrons ejected by protons for all the molecules we have studied except hydrogen. Data for a number of simple molecular targets are shown in Fig. 16 for 1.5 MeV proton impact. As in Fig. 9, we have scaled the cross sections compared in Fig. 16 by the number of weakly bound electrons. Scaled in this way, data for all molecules, except hydrogen, agree within experimental uncertainties. Had data for hydrocarbon molecules been included in the comparison (see for example, Wilson and Toburen, 1975) they would have shown slightly higher values at the peaks in the angular distributions, ie., somewhat more hydrogen-like, but when scaled in the same manner they would agree well with the molecules shown here at both large and small emission angles. If cross sections for higher ejected electron energies were plotted the peaks in the angular distributions would move to smaller angles in agreement with classical kinematics; ie., proportional to $\cos^2\theta$. Evidence of ionization via the CCT mechanism is seen as the increase in the cross sections

for the smallest angles of ejection and the highest energy electrons shown in Fig. 16. We would expect enhancement due to CCT to be most evident in distributions for ejected electron energies near 817 eV, an electron energy with equivalent velocity to the 1.5 MeV proton.

The most dramatic differences observed among the data shown in Fig. 16 is the large difference between the scaled molecular hydrogen cross sections and those of all the other molecules. Differences of more than an order of magnitude occur at both, small and large emission angle. This carries an even more important meaning when we recall that semi-classical and hydrogenic Born calculations yield results that mimic the hydrogen measurements, eg., see the binary encounter results shown in Fig. 14. It is only when realistic wave functions are used for both bound and continuum states that the Born approximation gives adequate agreement with measured doubly differential cross sections (Manson et al., 1975). Unfortunately techniques have not been developed for application of Born theory to molecular targets owing primarily to the unavailability of adequate wave functions. The general trends of the data shown are, of course, representative for fast collisions. An examination of the angular distributions for low-energy proton impact shown in Fig. 17 indicates that the distributions peak at zero degrees for all ejected electron energies (Cheng et al.,1989).

From a review of the doubly differential cross sections for electron emission by protons it would appear that the mechanisms responsible for ionization are well understood; this is particularly true for fast ions where the Born approximation in expected to be valid. Single differential cross sections for large energy losses can be described well by binary encounter theory and the

low-energy portion of the spectra is accurately evaluated using Bethe-Born theory combined with optical oscillator strengths and measured spectra to evaluate the hard collisions component of the cross sections. Where sufficient experimental data exists, the model of Rudd can be used to extrapolate cross sections over the complete range of proton energies. The angular distributions are not as fully understood. Binary encounter theory and hydrogenic Born calculations both underestimate the cross sections for emission of electrons into large and small angles. The similarity of angular distributions for a wide range of molecular targets, however, is conducive to the development of molecular models for use in track structure calculations. Charge-transfer-to-continuum states contributes to an enhancement of the cross sections for small emission angles, but does not contribute significantly to the total yield of electrons.

Structured Ion Impact

Studies of ionization of atomic and molecular targets by structured ion, ions that carry bound electrons and are sometimes referred to as clothed or dressed ions, have been underway for more than 20 years (see for example, Rudd et al., 1966; Cacak and Jorgensen, 1970; Wilson and Toburen, 1973) and have been discussed in reviews by Toburen (1989, 1982), Stolterfoht (1978, and Rudd (1975). Publications addressing doubly-differential cross sections for a broad range of collision partners are reviewed in table III of the appendix; in preparing this table an attempt was made to limit the publications included to those that involve measurement of absolute cross sections and that cover a reasonably wide range of ejected electron energies and angles.

The primary differences in the spectra of electrons ejected by ions that carry bound electrons from those ejected by bare ions can be seen in Fig. 18, where spectra are shown for ejection of electrons from water vapor by 0.3 MeV/amu H^+, He^{++}, and He^+ ions (Toburen et al., 1980); the proton data have been multiplied by a factor of 4 for comparison to the helium ion data. Note that the scaled proton data are in excellent agreement with the He^{++} results over most of the energy and angular range. This is representative of the accuracy of Z^2 projectile-charge scaling of collision cross sections for bare ions. The greatest differences between the scaled proton and bare helium ion cross sections occur at the smallest angles and for electron energies near 160 eV; this is the electron energy at which the electron and ion have comparable velocity. These differences are attributed to the CCT mechanism of ionization which has been predicted to have a Z^3 dependence on projectile charge (Dettman et al., 1974). In contrast to the excellent agreement between scaled H^+ and He^{++} cross sections the emission cross sections for He^+ impact exhibit marked differences from the bare ion results. Most evident is the reduction in cross section for ejection of low-energy electrons. These electrons are ejected in distant "soft" collisions in which the bound electron provides an effective electrostatic shield of the helium ion nucleus (Toburen et al., 1981). Higher energy electrons are ejected with increasingly close collisions that penetrate the shielding radius of the He^+ bound electron and are subject to the coulomb potential of the full nuclear charge, thus cross sections for high-energy electrons ejected in He^+ collisions are similar to those for He^{++} impact. In principal, one would expect a gradual change in the nature of the cross sections, from low-energy electrons that are ejected in large-impact parameter

collisions by what would appear to be a "heavy" proton, charge +1, to fast electrons ejected in close collisions by an effectively bare alpha particle, charge +2. Unfortunately the functional relationship that allows one to scale the charge as a function of energy loss, or impact parameter, has not been determined for different ions and molecular targets. The most obvious implication of the energy dependence of the "effective" nuclear charge is that the effective charge of stopping power theory, ie., an effective charge that is only a function of the nuclear charge and particle velocity, is totally inadequate for use in any theory of differential energy loss by dressed ions. The second feature of electron spectra for structured ions that is different from bare ions is the presence of a peak in the spectra from electrons that are stripped from the incident ion. These electrons are found predominantly in the forward directions, small emission angles in the laboratory reference frame, and at electron energies that correspond to electrons of the same velocity as the ion. Such a peak is visible in Fig. 18 in the 15- and 30-degree spectra at approximately 160 eV. In the 15-degree spectrum the contribution from projectile electron loss enhances the He^{+} spectrum over that for He^{++}. The contribution of electron loss from the projectile to the total yield of electrons con be demonstrated by plotting the ratio of the measured cross section to the Rutherford cross section as a function of 1/E as was described earlier; for comparison to heavier ions the Z^2 dependence of the Rutherford cross section must be implicitly included. Data for ionization of helium by 0.3 MeV/amu helium ions and protons are shown plotted in this way in Fig. 19. Excellent agreement between theory and experiment is observed between the H^{+} and He^{++} induced cross sections; the only differences are at electron energies less than about 18 eV (1/E=0.3) where one can expect larger

uncertainties in the helium ion data because no TOF data are available to improve the accuracy of the low-energy data. In these spectra the electron loss peak is clearly seen in the He^+ data; it enhances the cross sections well over those for bare ions in the region near electron energies of 160 eV ($1/\Sigma$=.07). The actual contribution of this process to the total ionization is, however, hard to determine because the effects of screening make identification of the portion of the curve due to target ionization difficult. One can see from this illustration, recalling that equal areas under the curve contribute equally to the total ionization cross section, that the mean energy of the ejected electrons will certainly be greater for He^+ ions than the bare ions.

Theoretical studies of structured ions have, until recently, been limited primarily to simple systems such as He^+-He (see DuBois and Manson, 1986, and references therein), although Stolterfoht and his colleagues have made a systematic study of the energy loss distributions in high energy neon ion collisions (Schneider et al., 1983). A comparison of the doubly-differential cross sections calculated with the Born approximation for the He^+-He collision system to spectra measured at 15 and 60 degrees with respect to the outgoing He^+ ion is shown in Fig. 20 (Manson and Toburen, 1981). Excellent agreement is observed for electrons ejected at 60 degrees, but differences of approximately a factor of 2 are found for the 15 degree spectra. Since the electrons are indistinguishable in these measurement it could not be determined whether the discrepancy resulted from calculation of target or projectile ionization. More recently measurement were made in which electrons were detected in coincidence with either the transmitted He^+ or stripped He^{++}

ion (DuBois and Manson, 1986). Those measurements demonstrated the inadequacy of the theoretical treatment to address simultaneous ionization processes, eg., ionization of both the projectile and target in a single collision. It is still not clear, however, whether the wave functions for the system are inadequate or if the discrepancies were a result of a breakdown in the Born approximation itself. Recently measurements have been undertaken for the H^0-He collision system (Heil et al., 1990) that now indicate that the Born approximation is adequate to describe these few electron systems if adequate wave functions are used for discrete and continuum states.

An example of the spectrum of electrons ejected in He^+ collisions with water vapor in which electrons are detected in coincidence with the stripped He^{2+} ion is shown in Fig. 21. One would expect the coincidence spectrum to be dominated by electrons lost by the projectile; a spectrum that peaks at approximately 400 eV for the ion energy considered. The expected spectrum of electrons stripped from the projectiles, based on the transformation of an ejected electron spectrum from the projectile frame of reference to the laboratory frame is shown as the dashed line in Fig. 21. The strong contribution of electrons at energies less than 400 eV is attributed to simultaneous projectile and target ionization. This simultaneous projectile and target ionization implies there will be a significant amount of correlation between the two ejected electron as they slow down in a biological medium. This could have impact on the subsequent chemical reactions that follow energy deposition.

Although a considerable amount of data has been generated for light structured ions, such as H^0, H_2^+, H_3^+, He^+, etc., and the features are relatively well understood in the high-energy range, there are only scattered sets of data for heavier ions and the theory of such collisions is only beginning to be developed. Because of their importance in neutron dosimetry we have initiated studies of electron emission for collisions involving carbon and oxygen ions. The relative contributions of the spectra of electrons from ionization of helium by H^+, He^+, and C^+ ions are shown in Fig. 22. Since these spectra are all scaled by Z^2 only the highest energy cross sections, produced by very close collisions, may be expected to scale to the same values; low-energy ejected electron cross sections reflect the extent of screening by the bound electrons. There is evidence of a small peak at the equal velocity condition, $v_e=v_i$, that occurs for R/E=0.07 indicating a small contribution resulting from electron loss from the C^+ ion. A comparison of spectra for different C^+ ion energies is shown in Fig. 23. This illustration shows that the electron loss contribution grows as the ion velocity increases reflecting the increasing electron-loss cross section. The most obvious characteristic of energy-loss in collisions of C^+ ions with atomic targets seen in Figs. 21 and 23 is the much lower fraction of low-energy electrons resulting from dressed ion collisions compared to bare ions. This leads to a much higher mean energy of the ejected electron in such collisions. Also note that it is not possible to scale proton cross sections to structured ion impact in any simple manner.

In the energy range where we have studied differential cross sections for carbon and oxygen ion impact, 66 to 350 keV/amu, the analysis advocated by Kim and discussed for protons in figs. 5 & 8, does not enable a test of the absolute

cross sections; there is no high energy plateau in the plot of Y(E,T) versus E. This is illustrated in Fig. 24. Absolute cross sections must, therefore be evaluated from experimental techniques and from recently measured total ionization cross sections (Reinhold et al., 1990; Toburen et al., 1990). Because of a combination of the effects of screening by projectile electrons and electron loss from the projectile it is difficult to identify the origin of the spectral features observed in Fig. 24. The peak , or shoulder for lower energy ions, at the low-energy end of the spectra is a result of electron loss from the projectile; the maximum contribution from this process for 4.2 MeV ions should be at about 190 eV (E/R=16). The electron loss peaks appear at a somewhat higher energy than predicted by kinematics because they are on a rapidly increasing background of electrons from target ionization. The binary encounter peak should be about 4 times higher in energy, or at approximately 58 Rydbergs for the 4.2 MeV spectrum. At this particle velocity one cannot expect a well defined binary encounter peak, see for example the proton impact data of Fig. 6.

The small peaks observed superimposed on the spectra for the two highest energy ions result from Auger transitions following inner-shell vacancy production in the carbon projectile. These transitions are observed at Doppler shifted energies in the laboratory determined by the kinematics of the collision. Since the spectra shown in Fig. 24 were obtained from integration of doubly-differential electron energy distributions measured at discrete angles these peaks carry forward as discrete peaks in the integral spectrum. The intensity of these transitions in the double differential cross sections also provides a means to determine the consistency of the measured absolute

cross sections and the energy scales by comparison to other measurements on inner-shell ionization.

There is presently very little information on the effects of projectile charge on the systematics of the doubly-differential ionization cross sections with the exception of studies undertaken for helium ions discussed earlier in this section. Measurements of doubly differential cross sections for collisions of 25 to 800 keV neon ions with neon by Woerlee, et al., (1981) showed little effect of a change in projectile charge from +1 to +3; the cross sections were reduced by about 10% per charge state independent of ejected electron energy. For these low energies the molecular promotion model is the primary mechanism of ionization and it would predict that the more electrons there are bound to the collision partners the more likely it is to promote a bound electron to a continuum state. For direct coulomb ionization, however, one would expect a more highly stripped ion to be more efficient at ejecting electrons from an atomic or molecular target. Cross sections for ejection of electrons from water vapor at 15 degrees with respect to outgoing oxygen ions of charge +1 to +3 are shown in Fig. 25. These data from our laboratory show the expected increase in cross section with projectile charge for ejection of low-energy electrons. They do not, however, increase as the square of the net projectile charge even for the lowest ejected electrons energies; these ejected in the most distant collisions. Thus, even at the largest impact parameters encountered in these measurements the ions do not appear as point charges. The data shown in Fig. 25 again illustrate the contribution to the spectra from electron loss by the projectile. This is the peak at $v_e=v_i$ that seems to decrease in intensity as the charge state increases reflecting the smaller

number of projectile electrons available to be stripped. The binary encounter peak from direct interactions between the incident oxygen nucleus and a target electron is also visible at about 400 eV. At the extreme high-energy end of the spectra is the Doppler shifted Auger electron spectra resulting from K-shell ionization of the oxygen projectile. Transitions of this type were responsible for the structure superimposed on the integral spectra shown in Fig. 24.

At the present time there is little theory that can help in the analysis and prediction of differential cross sections for structured ion. The Born approximation appears to adequately describe the collision for simple systems such as ionization by H^0 or He^+ ions if reliable wave functions are available for discrete and continuum states. This theory, however, appears a long way from application to more complex molecular systems of interest in Radiological Physics and, even where wave functions are available, the theory is usable only for high-energy ions. At the low-energy extreme, the use of a quasi-molecular description of the collision with electron promotion to the continuum via radial coupling has proven useful for modeling cross sections (Rudd, 1988; Woerlee et al. 1981). During the past few years Classical Trajectory Monte Carlo (CTMC) techniques have been developed for use in calculation of doubly differential cross sections for emission of electrons by intermediate and high energy ions (Schmidt et al., 1989; Reinhold et al., 1990). This technique is attractive in that it provides ab initio absolute cross sections and includes continuum charge transfer and multiple ionization processes, as well as being appropriate to the intermediate ion energy range. The primary disadvantage of this technique is the extraordinarily long

computational time required. In Fig. 26 is shown a recent calculation of the single differential cross sections for ejection of electrons in C^+ + He collisions at 200 keV/amu. There is good agreement between theory and experiment for the high energy portion of the spectra with the experimental data being about 50% larger than theory at the low energies. A strength of theory, as contrast to experiments, is that one is able to estimate the contribution, and the spectral shape, of electrons coming from either the target or the projectile. The dashed line in Fig. 26 is the calculated contribution of electrons ejected from the projectile. An example of the doubly-differential cross sections derived for this collision system is shown in Fig. 27. For this angle the experimental data are about 50% larger than the calculation; comparisons at smaller angles exhibit better agreement. Although there are discrepancies between the CTMC calculations and experiment, the agreement is comparable to, or better than, that seen earlier for Born calculations for simple collision systems, and the CTMC calculations can be applied to essentially any system as it does not rely on special system wave functions.

One could summarize our knowledge of differential ionization cross sections for structured ions as fragmentary. We have a reasonable understanding of collisions for light projectiles such as H^0 and He^+, although there is no theoretical means of calculating doubly-differential cross sections for molecular targets at the present time; neither have models been developed for fitting or extrapolating such cross sections. Data that exist, however, show dramatically that scaling from bare ions to dressed ions is not possible with a single parameter, such as the effective charge of stopping power theory, and

that the mean energy of electrons emitted in collisions involving structured ions is much higher that for bare ions. There is a long way to go before cross sections for structured ions will be understood with the same detail as bare ions, but recent advances in the development of theory and in experimental techniques give optimism to a vastly improved understanding in the near future.

Multiple Ionization and Charge Transfer

There is no question that the doubly-differential cross sections for electrons emission from charged particle impact are of primary importance in the development of track structure descriptions of energy deposition by high-LET radiation. However, the studies of electron emission do not provide any information regarding the fate of the target nor do they provide information on the number of electrons that may be emitted in a single collision. The latter may be biologically significant since the multiply emitted electrons would slow down in a spatially and temporally correlated way. To fully describe the interactions appropriate to a charged particle track one must have information on the charge transfer cross sections, the change in the spectrum of electrons emitted following charge transfer, the number of electrons emitted per interaction and their individual energy and angular distributions, and the excitation and dissociation states of the target molecules. To have detailed information on all of these processes, and the effect of target structure on them, is a tall order. As a first step, an assessment of the relative importance of the different processes can be very useful. For the past few years a part of our effort at PNL has been devoted

to measuring the spectrum of charge states of atomic and molecular products following ionizing collisions with light ions. These studies enable one to gain insight into the relative importance of different ionization channels appropriate to energy loss by ions and neutrals (see for example, DuBois, 1989, 1987a, 1987b, 1986, 1985, 1984; DuBois and Kover, 1989; DuBois and Toburen, 1988; and DuBois et al., 1984).

The principal interaction mechanisms leading to the release of free electron involving collisions of H^+ and He^+ ions with a neon target are illustrated in Fig. 28 for ion energies from a few keV/amu to a few hundred keV/amu. As expected, direct ionization is the primary source of electrons for proton collisions throughout the energy range. Electron capture, which requires simultaneous target ionization to release a free electron, is at most a 5% contributor to free electron production. For helium ion impact, however electron capture and loss can make a sizeable contribution to the free electron production. In the case of electron capture this implies a high probability of simultaneous capture-plus-target ionization leaving the target multiply ionized. It is also found that target ionization is produced with a high probability in collisions resulting in projectile ionization, although it is not obvious from this illustration. The message to be derived from this analysis is that, as projectiles heavier than protons are considered, processes other than direct ionization must by considered if electron production along the track is to be fully described.

In addition to electron capture-plus-projectile ionization that leaves the target atom doubly ionized it is also possible to produce a doubly ionized

target by direct ionization. The fraction of free electrons that result from multiple ionization of neon by protons and helium ions is shown in Fig. 29. This fraction never goes above 10% for proton impact, however for alpha particles the fraction approaches 100% at very low energies and is nearly 40% for He^+ ions over a large energy range. These data should remind us that one cannot simply scale data from protons to heavier ions. It should also encourage us to investigate the biological consequences of multiple ionization, ie., what are the effects of a transient build-up of localized coulomb charge. It is no doubt true that multiple ionization is less frequent in molecular and condensed phase targets, however, the difference in multiple ionization cross sections for different ions may be manifest as different molecular fragmentation patterns and yields that may be equally important in leading to biologically important damage. In the near future we should see an enhanced understanding of the relationship between the initial products of radiation and the subsequent chemistry and biology that is initiated. With the advances that are taking place in molecular biology the molecular view of radiation damage from energy deposition to biological expression is within our grasp.

Acknowledgements

Work supported by the Office of Health and Environmental Research (OHER), U.S. Department of Energy under Contract DE-AC06-76RLO 1830.

References

E. C. Beaty, K. H. Hesselbacher, S. P. Hong, and J. H. Moore, Measurements of the Triple-differential Cross Sections for low-Energy Electron-Impact Ionization of Helium, Phys. Rev. A 17:1592-1599 (1978).

J Berkowitz, Photoabsorption, Photoionization and Photoelectron Spectroscopy, (Academic Press, New York, 1979).

N. Bohr, The Penetration of Charged Particles through Matter, Det Kgl. Danske Videnskabernes Selskab. Mathematisk-fysiske Meddelelser XVIII, 8:1-143 (1947).

M. A. Bolorizadeh and M. E. Rudd, Angular and Energy Dependence of Cross Sections for Ejection of Electrons from Water Vapor. I. 50-2000-eV Electron Impact, Phys. Rev. A 33:882-887 (1986).

T. F. M. Bonson and L. Vriens, Angular Distribution of Electrons Ejected by Charged Particles I. Ionization of He and H_2 by Protons, Physica 47:307-319 (1970).

M. Breinig, S. B. Elston, S. Huldt, L. Liljeby, C. R. Vane, S. D. Berry, G. A. Glass, M. Schauer, I. A. Sellin, G. D. Alton, S. Datz, S. Overbury, R. Laubert, and M. Suter, Experiments Concerning Electron Capture and Loss to the Continuum and Convoy Electron Production by Highly Ionized Projectiles in the 0.7-8.5 MeV/amu Range Traversing the Rare Gases, Polycrystalline Solids and Axial Channels in Gold, Phys. Rev. A 25:3015-3048 (1982).

J. J. Butts and R. Katz, Theory of RBE for Heavy Ion Bombardment of Dry Enzymes and Viruses, Radiat. Res. 30:855-871 (1967).

R. K. Cacak and T. Jorgensen, Jr., Absolute Doubly Differential Cross Sections for Production of Electrons in Ne^+-Ne and Ar^+-Ar Collisions, Phys. Rev. A 2:1322-1327 (1970).

W. Chang, M. E. Rudd, and Y. Hsu, Differential Cross Sections for Ejection of Electrons from Rare Gases by 75-140 keV Protons, Phys. Rev. A 39:2359-2366 (1989).

D. E. Charlton, Calculation of Single and Double Strand DNA Breakage from Incorporated ^{125}I, in DNA Damage by Auger Emitters, Edited by K. F. Baverstock and D. E. Charlton (Taylor and Francis, New York, 1988) pp. 89-100.

A. Chatterjee and H. J. Shaefer, Microdosimetric Structure of Heavy Ion Tracks in Tissue, Rad. and Environm. Biophys. 13:215-227 (1976).

P. Cloutier and L. Sanche, A Trochoidal Spectrometer for the Analysis of Low-Energy Inelastically Backscattered Electrons, Rev. Sci. Instrum. 60:1054-1060 (1989).

J. B. Crooks and M. E. Rudd, Angular and Energy Distributions of Cross Sections for Electron Production by 50-300-keV Proton Impact on N_2, O_2, Ne, and Ar, Phys. Rev. A 3:1628-1634 (1971).

K. Dettman, K. G. Harrison, and M. W. Lucas, Charge Exchange to the Continuum for Light Ions in Solids, J. Phys. B 7:269-287 (1974).

M. Dillon, private communication (1990).

R. D. DuBois, Multiple Ionization of He^+-Rare-Gas collisions, Phys. Rev. A 39:4440-4450 (1989).

R. D. DuBois, Ionization and Charge Transfer in He^{2+}-Rare-Gas Collisions. II, Phys. Rev. A 36:2585-2593 (1987a).

R. D. DuBois, Recent Studies of Simultaneous Ionization and Charge Transfer in Helium Ion-Atom Collisions, Nucl. Instrum. Meth. B24/25:209213 (1987b).

R. D. DuBois, Ionization and Charge Transfer in He^{2+}-Rare Gas Collisions, Phys. Rev. A 33:1595-1601 (1986).

R. D. DuBois, Electron Production in Collisions Between Light Ions and Rare Gases: The Importance of the Charge-Transfer and Direct-Ionization Channels, Phys. Rev. Lett. 52:2348-2351 (1984).

R. D. DuBois and A. Kover, Single and Double Ionization of Helium by Hydrogen-Atom Impact, Phys. Rev. A 40:36053612 (1989).

R. D. DuBois and S. T. Manson, Coincidence Study of Doubly Differential Cross Sections: Projectile Ionization in He^+-He Collisions, Phys. Rev. Lett. 57:1130-1132 (1986).

R. D. DuBois and L. H. Toburen, Single and Double Ionization of Helium by Neutral-Particle to Fully Stripped Ion Impact, Phys. Rev. A 38:3960-3969 (1988).

R. D. DuBois, L. H. Toburen, and M. E. Rudd, Multiple Ionization of Rare Gases by H^+ and He^+ Impact, Phys. Rev. A 29:70-76 (1984).

M. Fujii, T Tamura, N. Mikami, and M. Ito, Electronic Spectra of Uracil in a Supersonic Jet, Chem. Phys. Lett. 126:583-587 (1986).

J. T. Grissom, R. N. Compton, and W. R. Garrett, Slow Electrons from Electron Impact Ionization of He, Ne, and Ar, Phys Rev. A 6:977-987 (1972).

O. Heil, R. Maier, M. Huzel, K.-O. Groeneveld, and R. D. DuBois, A Systematic Investigation of Ionization Occurring in Few Electron Systems, Phys. Rev. Lett., in press (1990).

S. P. Hong and E. C. Beaty, Measurements of the Triple-Differential Cross Sections for Low-Energy Electron-Impact Ionization of Argon, Phys. Rev A 17:1829 1836 (1978).

T. Inagaki, R. N. Hamm, and E. T. Arakawa, Optical and Dielectric Properties of DNA in the Extreme Ultraviolet, J. Chem. Phys. 61:4246-4250 (1974).

M. Inokuti, Introductory Remarks, IAEA-TECDOC-506 (International Atomic Energy Agency, Vienna, 1989) pp. 7-12 (1989).

Y.-K. Kim, Angular Distribution of Secondary Electrons in the Dipole Approximation, Phys. Rev. A 6:666-670 (1972).

Y.-K. Kim, Secondary Electron Spectra, in Radiation Research, Biomedical, Chemical, and Physical Prospectives, (Academic Press, Inc., New York, 1975) pp. 219-226.

Y.-K. Kim, Energy Distributions of Secondary Electrons I. Consistency of Experimental Data, Radiat. Res. 61:21-35 (1975a).

Y.-K. Kim and M. Inokuti, Slow Electrons Ejected by Fast Charged Particles, Phys. Rev. A 7:1257-1260 (1973).

Y.-K. Kim and T. Noguchi, Secondary Electrons Ejected from He by Protons and Electrons, Int. J. Radiat. Phys. Chem. 7:77-82 (1975).

D. E. Lea, Actions of Radiation on Living Cells (The Macmillan Company, New York, 1947).

D. J. Lynch, L. H. Toburen, and W. E. Wilson, Electron Emission from Methane, Ammonia, Monomethylamine and Dimethylamine by 0.25 to 2.0 MeV Protons, J. Chem. Phys. 64:2616-2622 (1976).

J. Macek, Theory of the Forward Peak in the Angular Distribution of Electrons Ejected by Fast Protons, Phys. Rev. A 1:235-241 (1970).

D. H. Madison, Angular Distribution of Electrons Ejected from Helium by Proton Impact, Phys. Rev. A 8:2449-2456 (1973).

S. T. Manson and L. H. Toburen, Energy and Angular Distributions of Electrons from Fast He^++He Collisions, Phys. Rev Lett. 46:529-531 (1981).

S. T. Manson, L. H. Toburen, D. H. Madison, and N. Stolterfoht, Energy and Angular Distributions of Electrons Ejected from Helium by Fast Protons and Electrons: Theory and Experiment, Phys. Rev. A 12:60-78 (1975).

R. M. Marsolais and L. Sanche, Mechanisms Producing Inelastic Structures in Low-Energy Electron Transmission Spectra, Phys. Rev. B 38:11 118-11 130 (1988).

E. W. McDaniel, M. R. Flannery, E. W. Thomas, H. W. Ellis, K. J. McCann, S. T. Manson, J. W. Gallagher, J. R. Rumble, E. C. Beaty, and T. G. Roberts, Compilation of Data Relevant to Nuclear Pumped Lasers, Vol. V, Technical Report H-78-1 (US Army Missile Research and Development Command, Redstone Arsenal, Alabama, 1979) pp. 1917-2011.

M. Michaud and L. Sanche, Total Cross Sections for Slow-Electron (1-20 eV) scattering in solid H_2O, Phys. Rev. A 36:4672-4683 (1987).

J. H. Miller and S. T. Manson, Differential Cross Sections for Ionization of Helium, Neon, and Argon by Fast Electrons, Phys. Rev. A 29:2435-2439 (1984).

J. H. Miller, L. H. Toburen, and S. T. Manson, Differential Cross Sections for Ionization of Helium, Neon, and Argon by High-Velocity Ions, Phys. Rev. A 27:1337-1344 (1983).

J. H. Miller, W. E. Wilson, S. T. Manson, and M. E. Rudd, Differential Cross Sections for Ionization of Water Vapor by High-Velocity Bare Ions and Electrons, J. Chem. Phys. 86:157-162 (1987).

N. Oda, Energy and Angular Distributions of Electrons from Atoms and Molecules by Electron Impact, Radiat. Res. 64:80-95 (1975).

C. E. Opal, W. K. Peterson, and E. C. Beaty, Measurements of Secondary-Electron Spectra Produced by Electron Impact Ionization of a Number of Simple Gases, J. Chem. Phys. 55:4100-4106 (1971).

H. G. Paretzke, Radiation Track Structure Theory, in Kinetics of Nonhomogeneous Processes, ed. by G. R. Freeman (John Wiley and Sons, New York, 1987) pp. 89-170.

C. O. Reinhold, D. R. Schultz, R. E. Olson, L. H. Toburen, and R. D. DuBois, Electron Emission from Both Target and Projectile in C^+ + He Collisions, J. Phys. B 23:L297-L302 (1990).

3.B. Robinson, Modifications of the Impulse Approximation for Ionization and Detachment Cross Sections, Phys. Rev. 140:A764-768 (1965).

1. E. Rudd, Mechanisms of Electron Production in Ion-Atom Collisions, Radiat. Res. 64:153-180 (1975).

1. E. Rudd, Energy and Angular Distributions of Electrons from 5-100-keV-Proton Collisions with Hydrogen and Nitrogen Molecules, Phys. Rev. A 20:787-796 (1979).

1. E. Rudd, Differential Cross Sections for Secondary Electron Production by Proton Impact, Phys. Rev. A 38:6129-6137 (1988).

1. E. Rudd, T. Jorgensen, Jr. and D. J. Volz, Electron Energy Spectra from Ar^+-Ar and H^+-Ar Collisions, Phys. Rev 151:28-31 (1966).

1. E. Rudd, Y.-K. Kim, D. H. Madison, and J. W. Gallagher, Electron Production n Proton Collisions: Total Cross Sections, Rev. Mod. Phys. 57:965-994 (1985).

. Sanche, Investigation of Ultra-Fast Events in Radiation Chemistry with Low-nergy Electrons, Radiat. Phys. Chem. 34:15-33 (1989).

S. Schmidt, J. Euler, C. Kelbch, S. Kelbch, R. Koch, G. Kraft, R. E. Olson, U. Ramm, J. Ullrich, and H. Schmidt-Bocking, Double Differential Stopping of 1.4 Mev/amu U^{33+} in Ne and Ar Derived from Electron Production and Multiple Ionization Cross Sections, Technical report number GSI-89-19 (Gesellschaft fur Schwerionenforschung, Darmstadt, Germany, 1989).

D. Schneider, M. Prost, N Stolterfoht, G. Nolte, and R. D. DuBois, Projectile Ionization in Fast Heavy Ion-Atom Collisions, Phys Rev. A 28:649-655 (1983).
B. L. Schram, F. J. de Heer, M. J. van de Wiel and J. Kistemaker, Ionization Cross Sections for Electrons (0.6-20keV) in Noble and Diatomic Gases, Physica 31:94-112 (1965).

I. Shimamura, Cross Sections for Collisions of Electrons with Atoms and Molecules, Scientific Papers of the Institute of Physical and Chemical Research (Japan) 82:1-50 (1989).

W. Sontag and F. Weibezahn, Absorption of DNA in the Region of Vacuum-uv, Rad. and Environm. Biophys. 12:169-174 (1975).

N. Stolterfoht, Angular and Energy Distributions of Electrons Produced by 200-500 keV Protons in Gases: I. Experimental Arrangement, Z. Phys. 248:81-93 (1971).

N. Stolterfoht, Excitation in Energetic Ion-Atom Collisions Accompanied by Electron Emission, in Topics in Current Physics V.: Structure and Collisions of Ions and Atoms, ed by I. A. Sellin (Springer-Verlag,Berlin, 1978) pp. 155-199.

L. H. Toburen, Distributions in Energy and Angle of Electrons Ejected from Molecular Nitrogen by 0.3-1.7 MeV Protons, Phys. Rev. A 3:216-227 (1971).

L. H. Toburen, Continuum Electron Emission in Heavy-Ion Collisions, in Nuclear Methods 2; High-Energy Ion-Atom Collisions, ed. by D. Brenyi and G. Hock (Elsever, New York, 1982) pp. 53-82.

L. H. Toburen, Atomic and Molecular Processes of Energy Loss by Energetic Charged Particles, IAEA-TECDOC-506 (International Atomic Energy Agency, Vienna, 1989) pp. 160-168 (1989).

L. H. Toburen and W. E. Wilson, Time-of-Flight measurements of Low-Energy Electron Energy Distributions from Ion-Atom Collisions, Rev. Sci. Instrum. 46:851-854 (1975).

L. H. Toburen and W. E. Wilson, Secondary Electron Emission in Ion-Atom Collisions, in Radiation Research, ed by S. Okada, M. Imamura, T. Terashima, and H. Yamaguchi (Toppan Printing Co., Tokyo, 1979) pp. 80-88.

L. H. Toburen, S. T. Manson, and Y.-K. Kim, Energy Distributions of Secondary Electrons. III. Projectile Energy Dependence for Ionization of He, Ne, and Ar by Protons, Phys. Rev. A 17:148-159 (1978).

L. H. Toburen, W. E. Wilson, and R. J. Popowich, Secondary Electron Emission from Ionization of Water Vapor by 0.3- to 2.0-MeV He^{+} and He^{++} Ions, Radiat. Res. 82:27-44 (1980).

L. H. Toburen, N. Stolterfoht, P. Ziem, and D. Schneider, Electronic Screening in Heavy-Ion Collisions, Phys. Rev. A 24:1741-1745 (1981).

L. H. Toburen, R. D. DuBois, C. O. Reinhold, D. R, Schultz, and R. E. Olson, Experimental and Theoretical Study of the Electron Spectra in 66.7 to 350 keV/amu C^{+} + He Collisions, Phys. Rev. A , In Press (1990).

W. E. Wilson and L. H. Toburen, Electron Emission in H_2^{+}-H_2 Collisions from 0.6 to 1.5 MeV, Phys. Rev. A 7:1535-1544 (1973).

W. E. Wilson and L. H. Toburen, Electron Emission from Proton-Hydrocarbon-Molecule Collisions, Phys. Rev. A 11:1303-1308 (1975).

W. E. Wilson, J. H. Miller, L. H. Toburen, and S. T. Manson, Differential Cross Sections for Ionization of Methane, Ammonia, and Water Vapor by High Velocity Ions, J. Chem. Phys. 80:5631-5638 (1984).

P. H. Woerlee, Yu. S. Gordeev, H de Waard, and F. W. Saris, The Production of Continuous Electron Spectra in Collisions of Heavy Ions and Atoms. B: Direct Coupling with the Continuum, J. Phys. B 14:527-539 (1981).

Figure Captions

Fig. 1. Simulated 2 MeV alpha particle track compared to spatial patterns of DNA structures, A: comparison to linker and nucleosomes structures, the distance between the two (+) markers is 10 nm; B: an end-on view of the same track segment as in A; C: a portion of the same track magnified to the dimensions comparable to the atomic positions of DNA, the distance between the two (+) markers is 10 Å.

Fig. 2. Angular distributions of electrons ejected from water vapor by 500 eV electron impact. The data are from (+) Opal et al. (1971), (■) Oda (1975), and (o) Bolorizadeh and Rudd (1986).

Fig. 3. Secondary electron spectra for electron impact ionization of N_2. The areas under the curves have been normalized to the respective total ionization cross sections. The area between the shaded lines corresponds to the fraction of the electrons ejected with insufficient energies to produce further ionization in the target medium. These data of Kim (1975) were reproduced with permission of the author.

Fig. 4. Comparison of absolute cross sections for ionization of N_2 by 0.3 MeV protons measured by (●) Stolterfoht (1971), (o) Crooks and Rudd (1971), and (x) Toburen (1971), and the relative line shape for low-energy ejected electrons measured by TOF techniques (Toburen and Wilson, 1975).

Fig. 5. The ratio of the measured singly-differential cross section for proton ionization of helium (Toburen et al., 1978) to the Rutherford cross section.

Fig. 6. The ratio of the measured singly-differential cross section to the Rutherford cross sections for ionization of neon by protons.

Fig. 7. The ratio of the measured to Rutherford singly-differential cross sections for ionization of a number of molecules by protons, data of Lynch et al., (1976).

Fig. 8. Comparison of measured and calculated singly-differential cross sections for ionization of neon by 1.0 MeV protons; cross sections are presented as the ratio to the Rutherford cross section for outer-shell ionization of neon. The measured single differential cross sections (x) are from Toburen et al. (1978). The cross section for zero energy ejected electrons (□) is from Grissom (1972). The binary encounter calculations are from a program of Rudd (1975) and includes results assuming the average kinetic energy of the bound electron is equal to the binding energy (BE_I) or given by Slater's rules (BE_S). The Rutherford cross section is calculated including inner-shell contributions (Kim, 1975) and the Plane wave Born Calculation (Δ) is described by Toburen et al., (1978).

Fig. 9. Singly-differential cross sections for ionization of several molecules by 1 MeV protons.

Fig. 10. Ratio of the measured singly-differential cross sections to the corresponding Rutherford values plotted as a function of 1/energy loss for ionization of neon by protons and electrons. The electron results are from Opal et al. (1971) and the proton data are from Toburen et al., (1978).

Fig. 11. The hard collision component of the Bethe-Born cross section, B(E), for ionization of water vapor by protons.

Fig. 12. Singly-differential cross sections from the model of Miller (1983) compared to measurements for ionization of water vapor by protons.

Fig. 13. The calculated singly-differential cross sections (solid lines) for ionization of N_2 by protons from the model of Rudd (1988) compared to the experimental data of (o) Rudd (1979), (•) Crooks and Rudd (1971), (x) Toburen (1971), and (□) Stolterfoht (1971).

Fig. 14. Doubly-differential cross sections for ionization of helium by 2 MeV protons. The binary encounter theory calculation (BEA) is from Bonson and Vriens (1970) and the plane wane Born approximation is from the work of Madison (1973).

Fig. 15. Doubly differential cross sections for emission of electrons of velocity comparable to the projectile compared to calculations of Macek (1971) and the plane wave Born approximation.

Fig. 16. Doubly-differential cross sections measured at PNL for ionization of a number of molecules by 1.5 MeV protons all scaled according to the number of loosely bound electrons.

Fig. 17. Angular distributions of electrons of several energies ejected from krypton by low energy protons; this figure was reproduced from Cheng et al. (1989).

Fig. 18. Doubly differential cross sections for electron emission from water vapor by 0.3 MeV/amu protons and helium ions. The proton data have been multiplied by 4 (as implied by Z^2 scaling) for comparison to the helium ion results; the data are from Toburen et al. (1980).

Fig. 19. Ratio of the measured singly-differential cross sections for ionization of helium by 0.3 MeV/amu protons and helium ions to the corresponding Rutherford cross sections.

Fig. 20. Comparison of the doubly-differential cross sections for ionization of helium by 2 MeV He^+ to calculations based on the Born approximation (Manson and Toburen, 1981).

Fig. 21. Comparison of the spectrum of electrons detected in coincidence with ionization of the He^+ projectile to that of all electrons ejected at 20 degrees with respect to the exiting ion.

Fig. 22. Comparison of the singly differential cross sections for ionization of helium by 0.3 MeV/amu H^+, He^+, and C^+ ions plotted as the ratio to the corresponding Rutherford cross sections.

Fig. 23. The ratio of measured and Rutherford cross sections for ionization of helium by singly-charged carbon ions plotted as a function of the inverse of the energy loss.

Fig. 24. The ratio of measured and Rutherford cross sections for ionization of helium by singly charged carbon ions plotted as a function of the energy loss.

Fig. 25. Doubly differential cross sections for ionization of water vapor by oxygen ions of different charge states. Arrows point out the position of the KLL-Auger spectrum resulting from relaxation of K-shell vacancies produced in the oxygen projectile, the binary peak (BEP) for electrons originating from the target, and the electron loss peak ($v_e = v_i$) of electrons originating from the projectile.

Fig. 26. Comparison of measured singly-differential cross sections for ionization of helium by C^+ to the classical trajectory Monte Carlo (CTMC) calculation of Reinhold et al. (1990).

Fig. 27. Comparison of measured doubly differential cross sections for emission of electrons at 50 degrees by C^+ ions to classical trajectory Monte Carlo (CTMC) calculations of Reinhold et al. (1990).

Fig. 28. Comparison of the relative importance of the principal mechanisms for production of free electrons in collisions of protons and helium ions with neon.

Fig. 29. Comparison of the fractions of free electrons produced from multiple ionization events for protons and helium ions colliding with neon atoms.

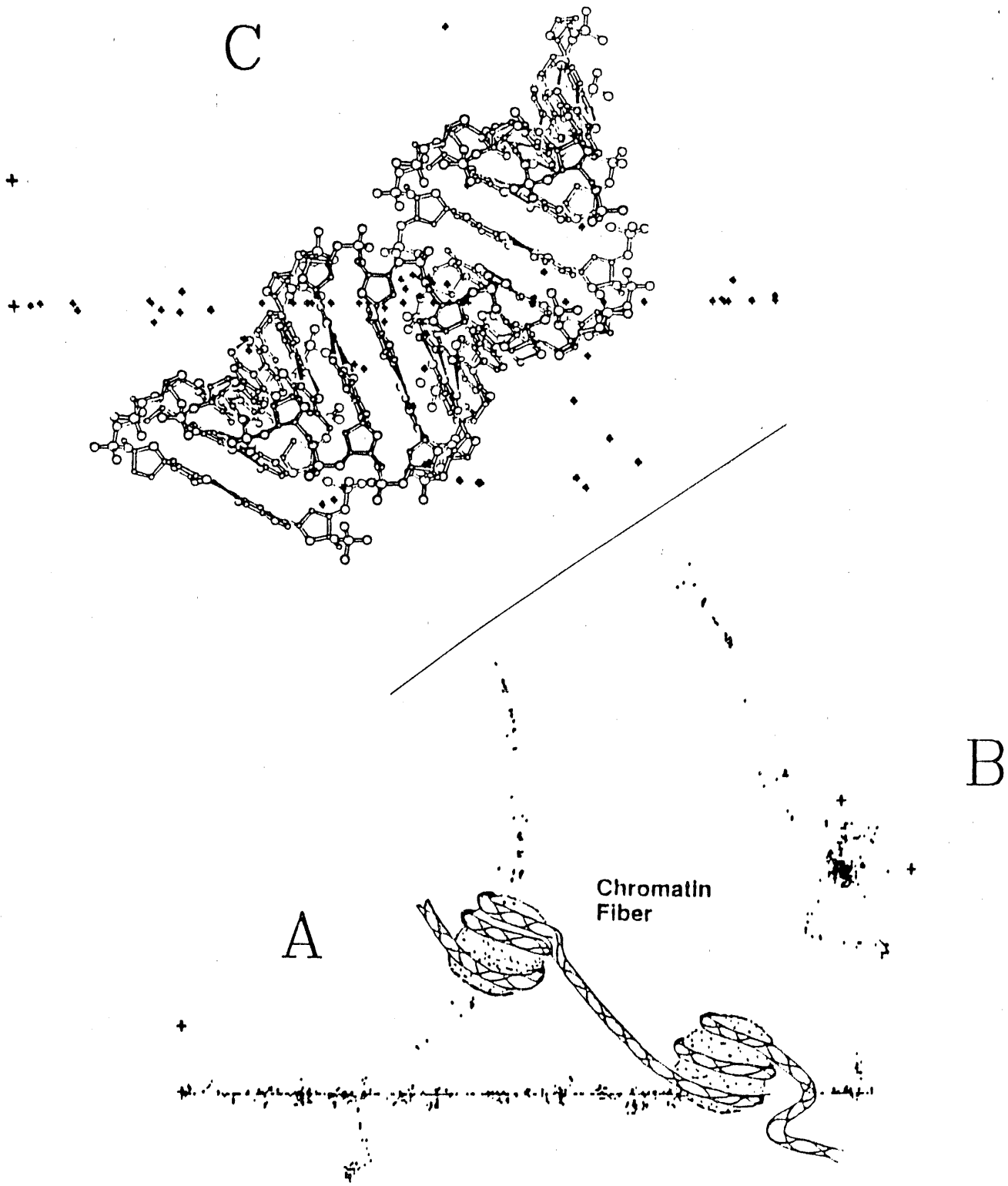

FIGURE 1

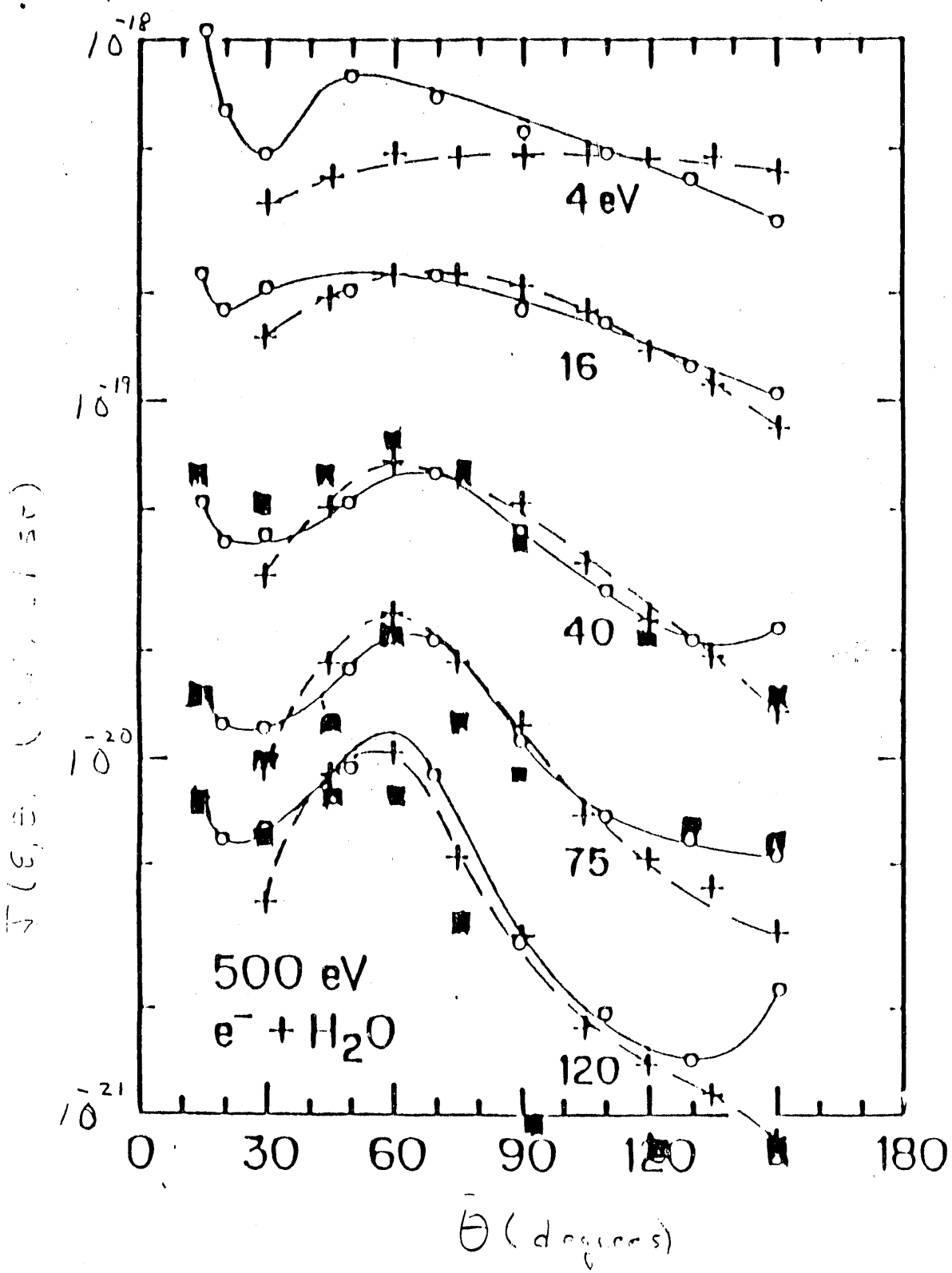
10^{-18}
4 eV
16
10^{-19}
40
10^{-20}
75
500 eV
$e^- + H_2O$
120
10^{-21}
0
30
60
90
120
180
θ (degrees)

FIGURE 2

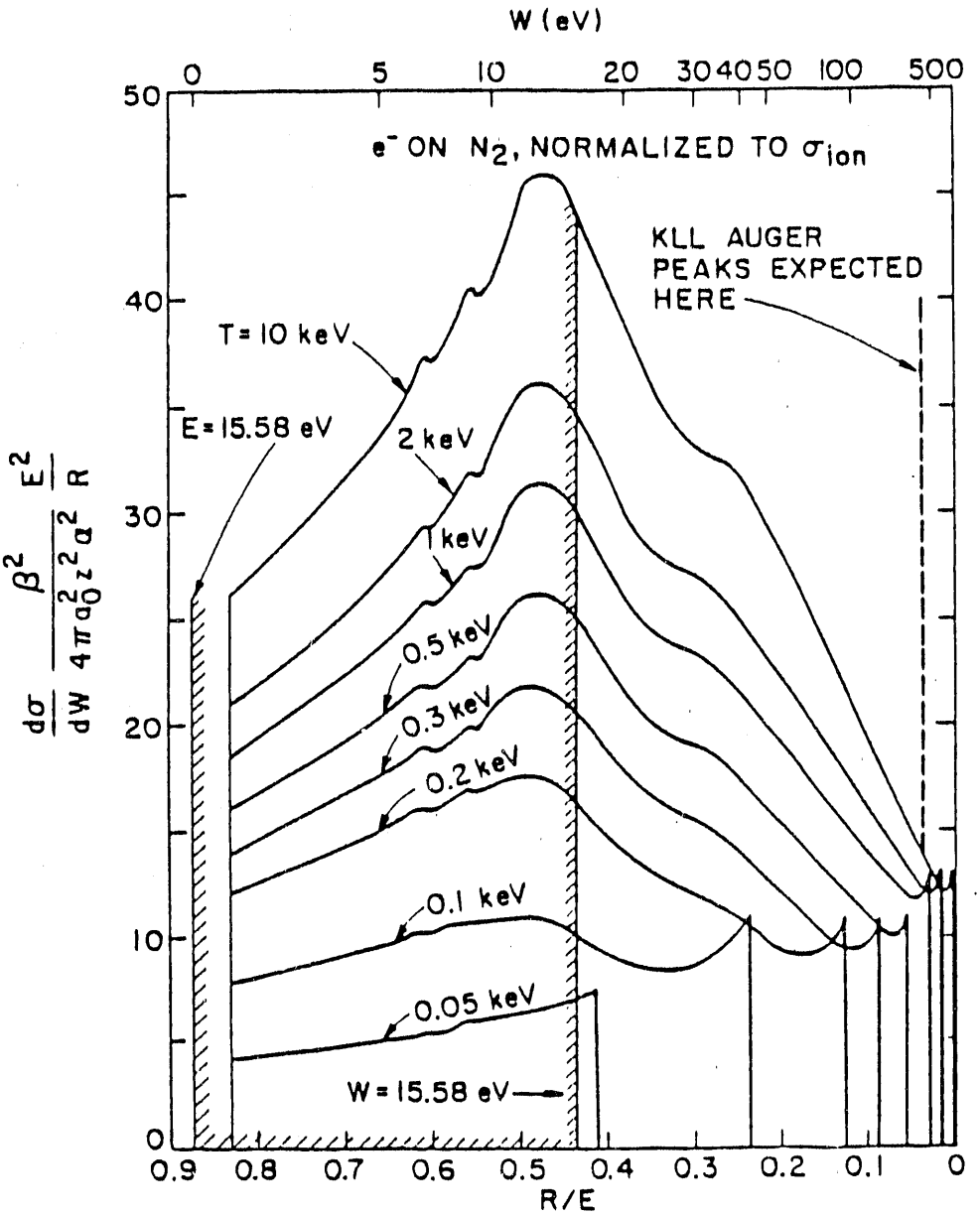
W (eV)
0
5
10
20
30
40
50
100
500
e⁻ ON N2, NORMALIZED TO σion
KLL AUGER PEAKS EXPECTED HERE
T = 10 keV
E = 15.58 eV
2 keV
1 keV
0.5 keV
0.3 keV
0.2 keV
0.1 keV
0.05 keV
W = 15.58 eV
dσ/dW β²/(4πa0²z²α²) E²/R
50
40
30
20
10
0
0.9
0.8
0.7
0.6
0.5
0.4
0.3
0.2
0.1
0
R/E

FIGURE 3

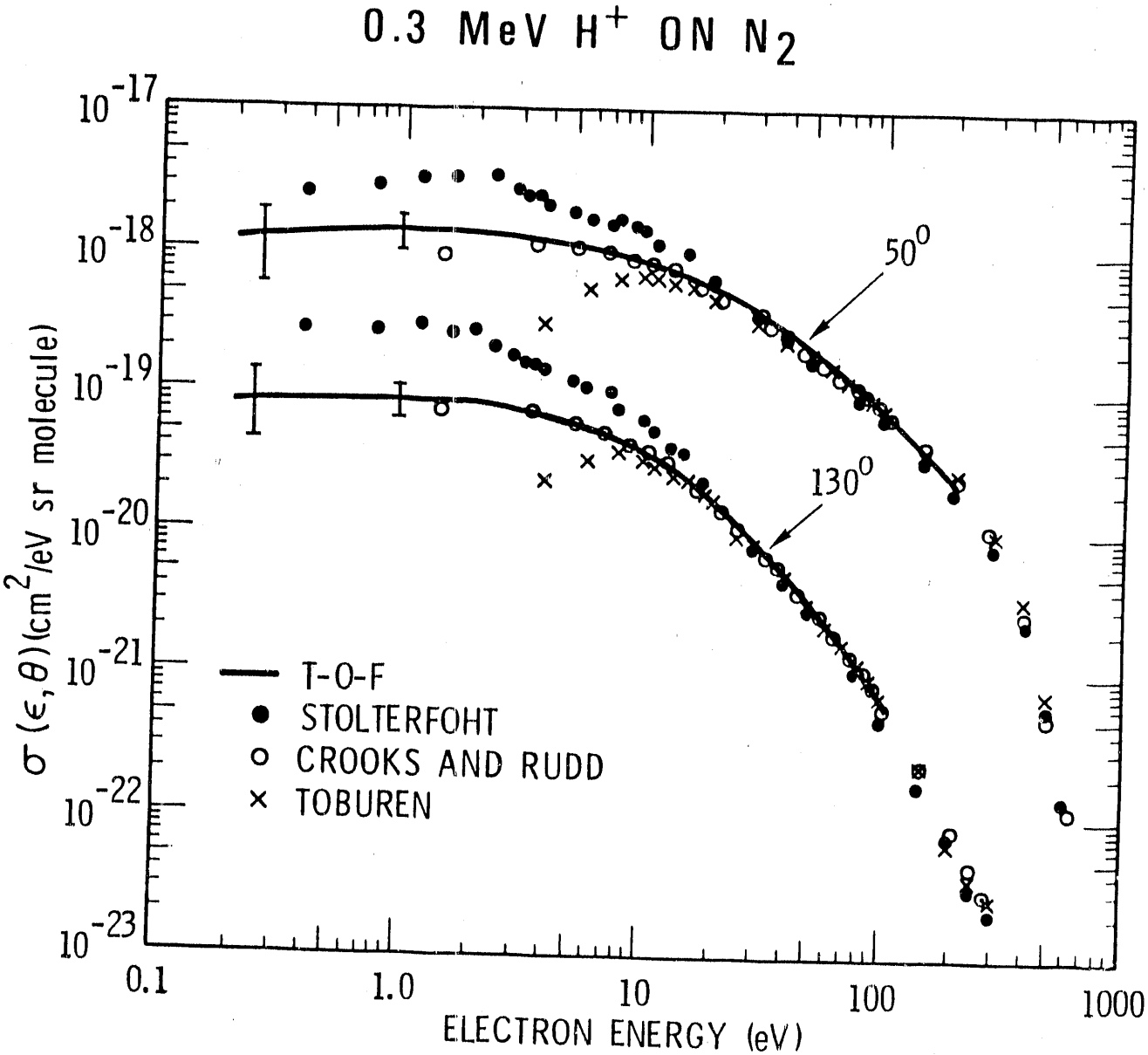
0.3 MeV H+ ON N2
10-17
10-18
10-19
10-20
10-21
10-22
10-23
σ (ϵ, θ)(cm2/eV sr molecule)
50°
130°
T-O-F
STOLTERFOHT
CROOKS AND RUDD
TOBUREN
0.1
1.0
10
100
1000
ELECTRON ENERGY (eV)

FIGURE 4

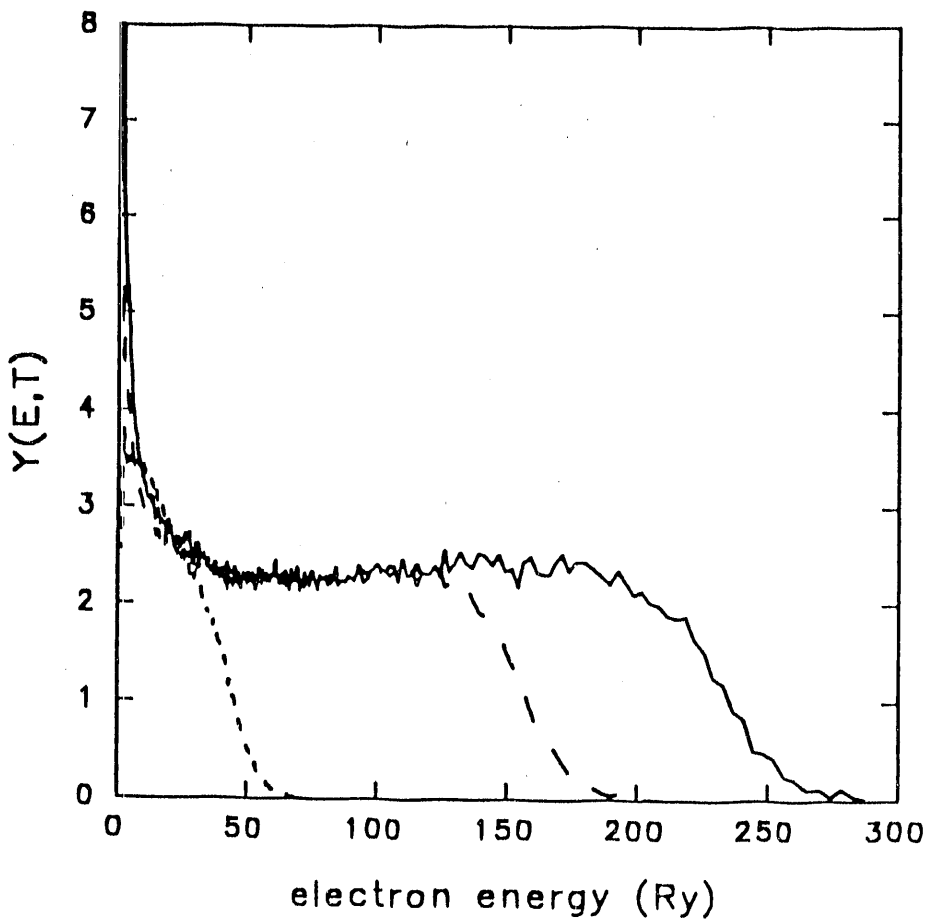

FIGURE 5

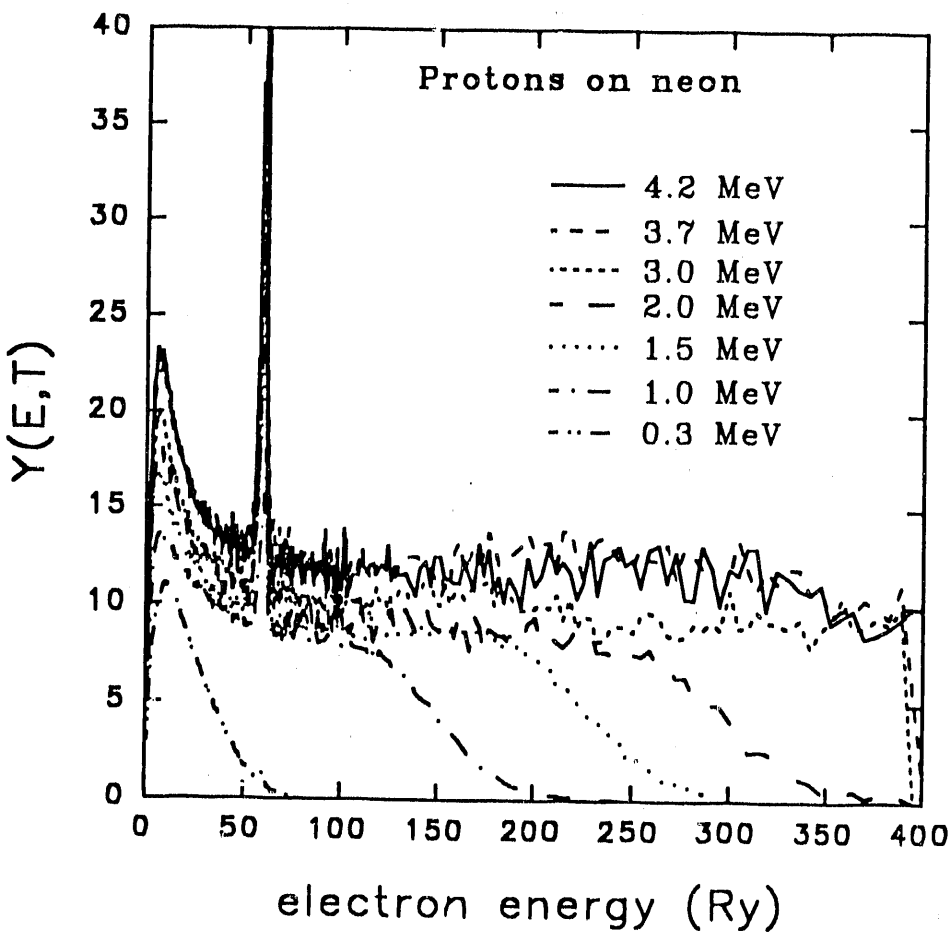
Protons on neon
4.2 MeV
3.7 MeV
3.0 MeV
2.0 MeV
1.5 MeV
1.0 MeV
0.3 MeV
Y(E,T)
electron energy (Ry)
0
5
10
15
20
25
30
35
40
0
50
100
150
200
250
300
350
400

FIGURE 6

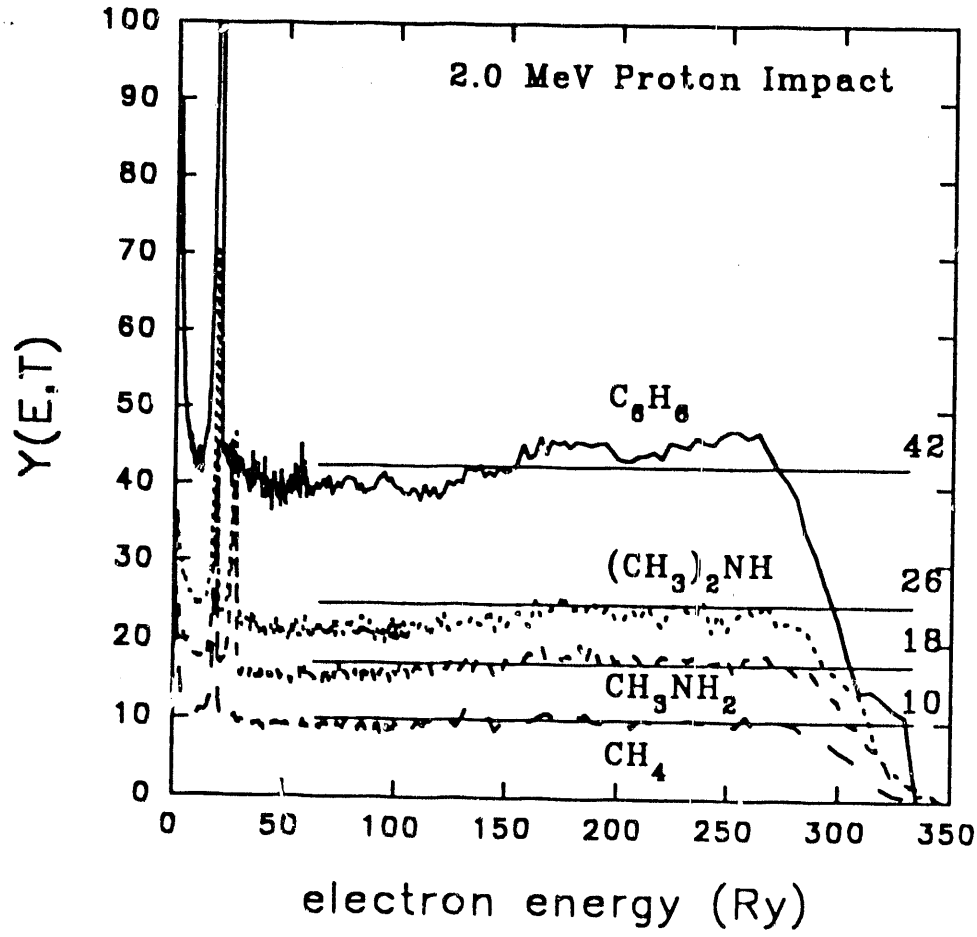
2.0 MeV Proton Impact
Y(E,T)
electron energy (Ry)
C_6H_6
$(CH_3)_2NH$
CH_3NH_2
CH_4
42
26
18
10
0
10
20
30
40
50
60
70
80
90
100
0
50
100
150
200
250
300
350

FIGURE 7

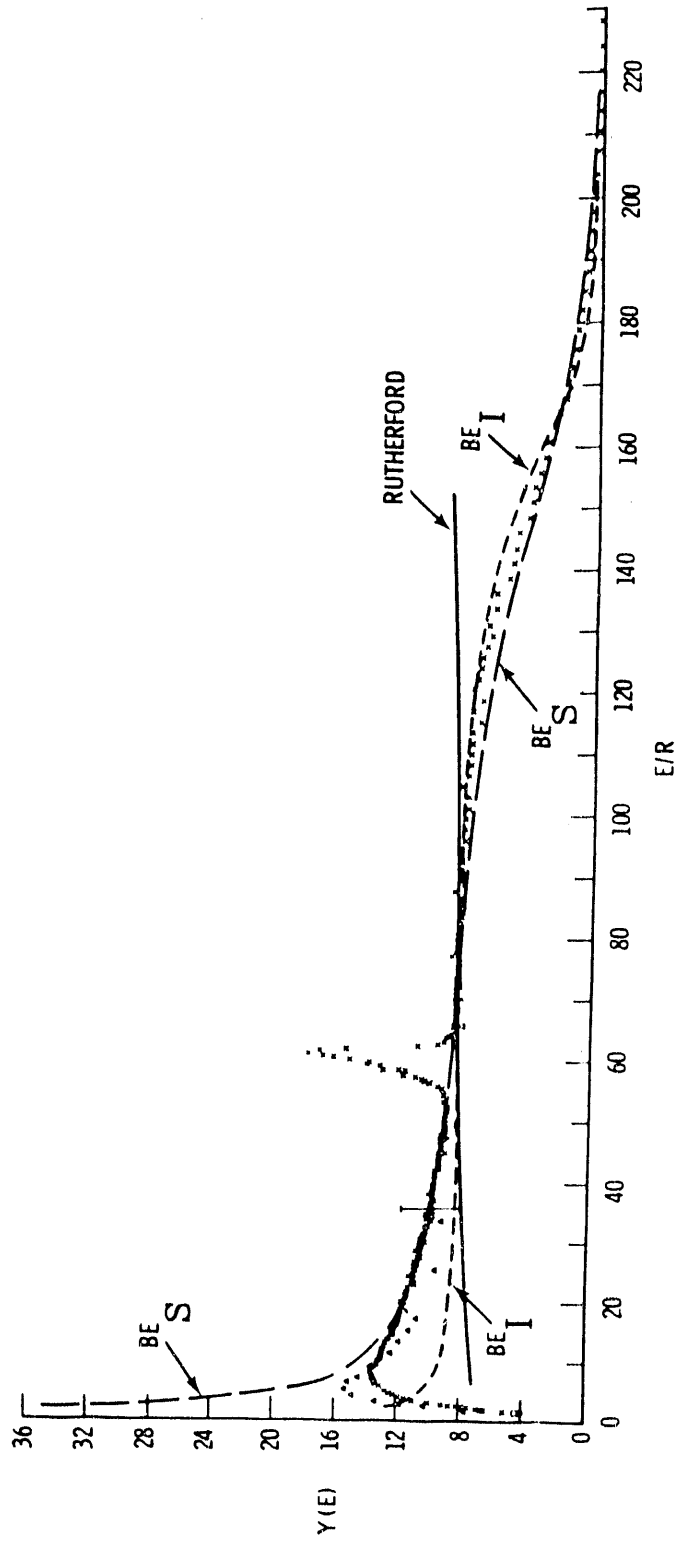
RUTHERFORD
BE S
BE I
BE S
BE I
Y(E)
E/R
0
4
8
12
16
20
24
28
32
36
0
20
40
60
80
100
120
140
160
180
200
220

FIGURE 8

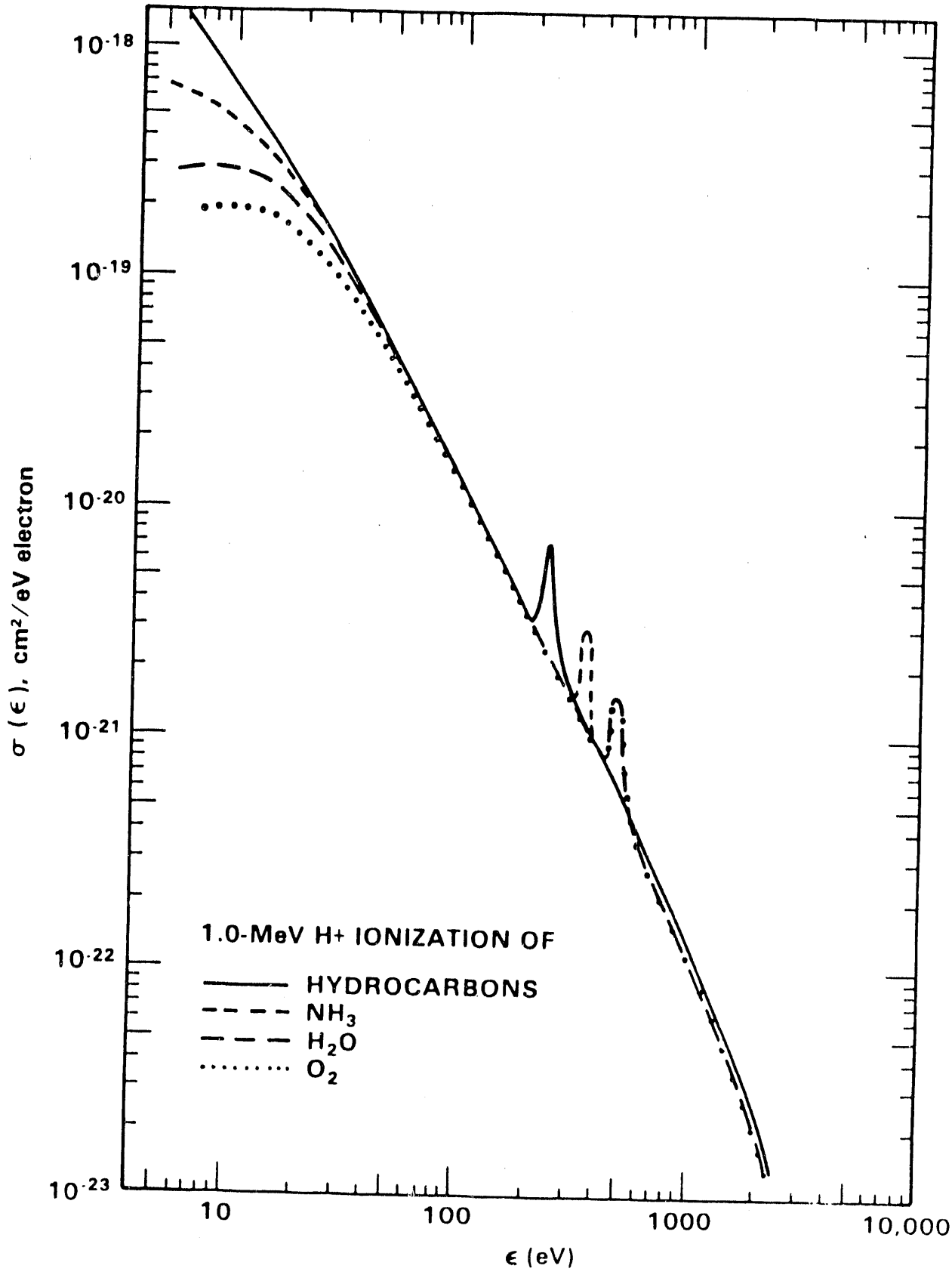
10^{-18}
10^{-19}
10^{-20}
10^{-21}
10^{-22}
10^{-23}
$\sigma(\epsilon)$, cm²/eV electron
10
100
1000
10,000
ϵ (eV)
1.0-MeV H+ IONIZATION OF
HYDROCARBONS
NH_3
H_2O
O_2

FIGURE 9

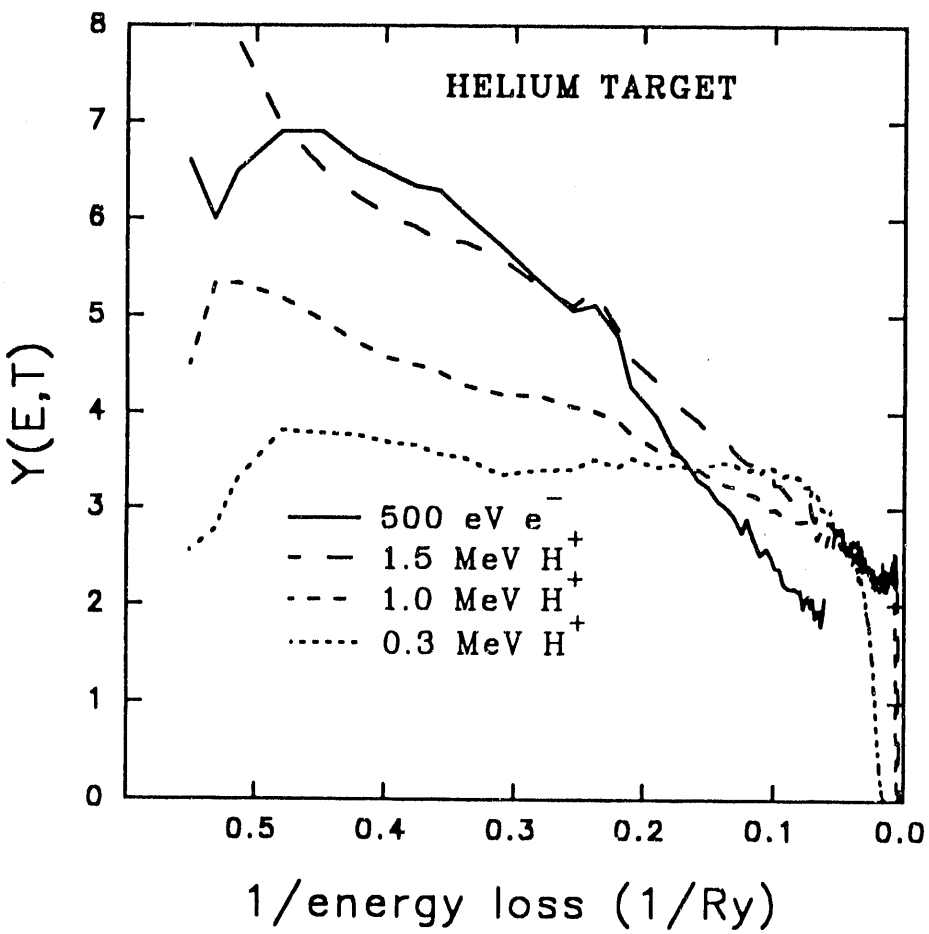
HELIUM TARGET
Y(E,T)
1/energy loss (1/Ry)
500 eV e⁻
1.5 MeV H⁺
1.0 MeV H⁺
0.3 MeV H⁺
0
1
2
3
4
5
6
7
8
0.5
0.4
0.3
0.2
0.1
0.0

FIGURE 10

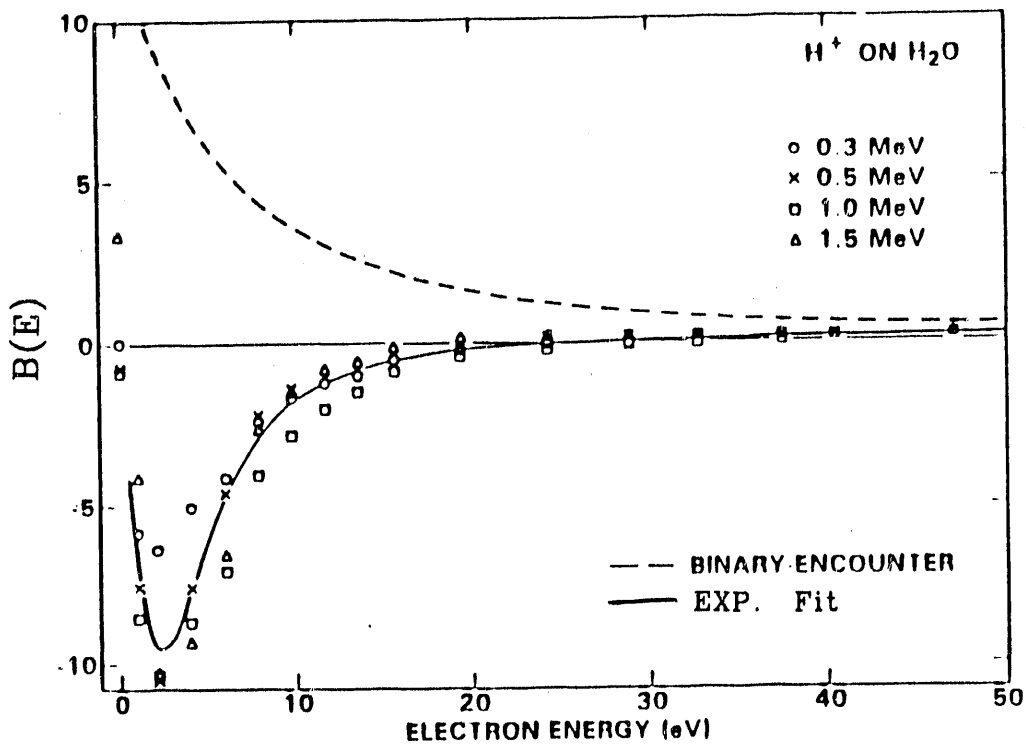
H^+ ON H_2O
o 0.3 MeV
× 0.5 MeV
□ 1.0 MeV
△ 1.5 MeV
— — BINARY ENCOUNTER
—— EXP. Fit
B(E)
ELECTRON ENERGY (eV)
10
5
0
-5
-10
0
10
20
30
40
50

FIGURE 11

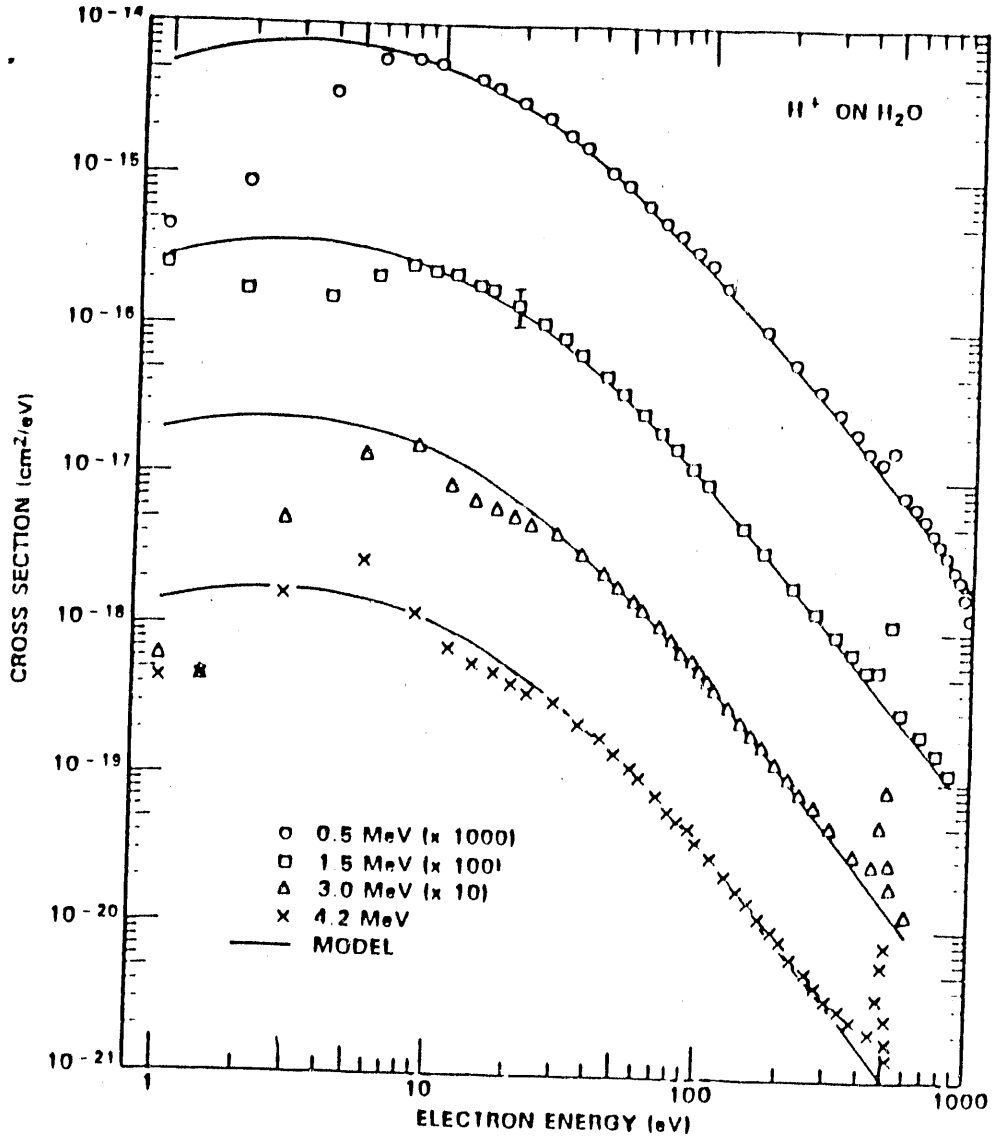
H^+ ON H_2O
CROSS SECTION (cm^2/eV)
10^{-14}
10^{-15}
10^{-16}
10^{-17}
10^{-18}
10^{-19}
10^{-20}
10^{-21}
1
10
100
1000
ELECTRON ENERGY (eV)
0.5 MeV (x 1000)
1.5 MeV (x 100)
3.0 MeV (x 10)
4.2 MeV
MODEL

FIGURE 12

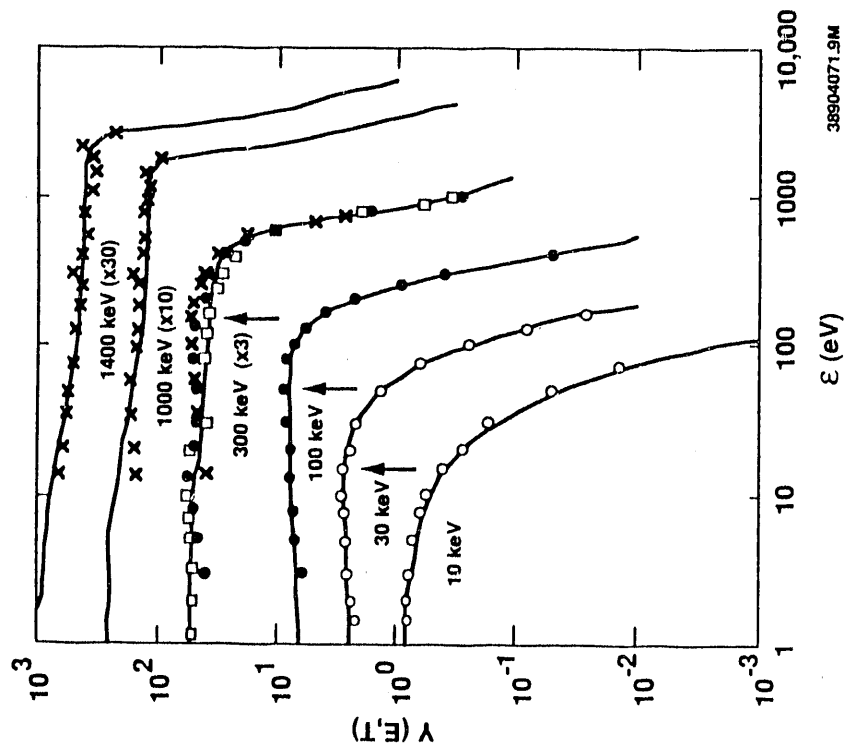
1400 keV (x30)
1000 keV (x10)
300 keV (x3)
100 keV
30 keV
10 keV
Y (E,T)
ε (eV)
10,000
1000
100
10
1
10^3
10^2
10^1
10^0
10^-1
10^-2
10^-3
38904071.9M

FIGURE 13

2.0 MeV H^+ ON He

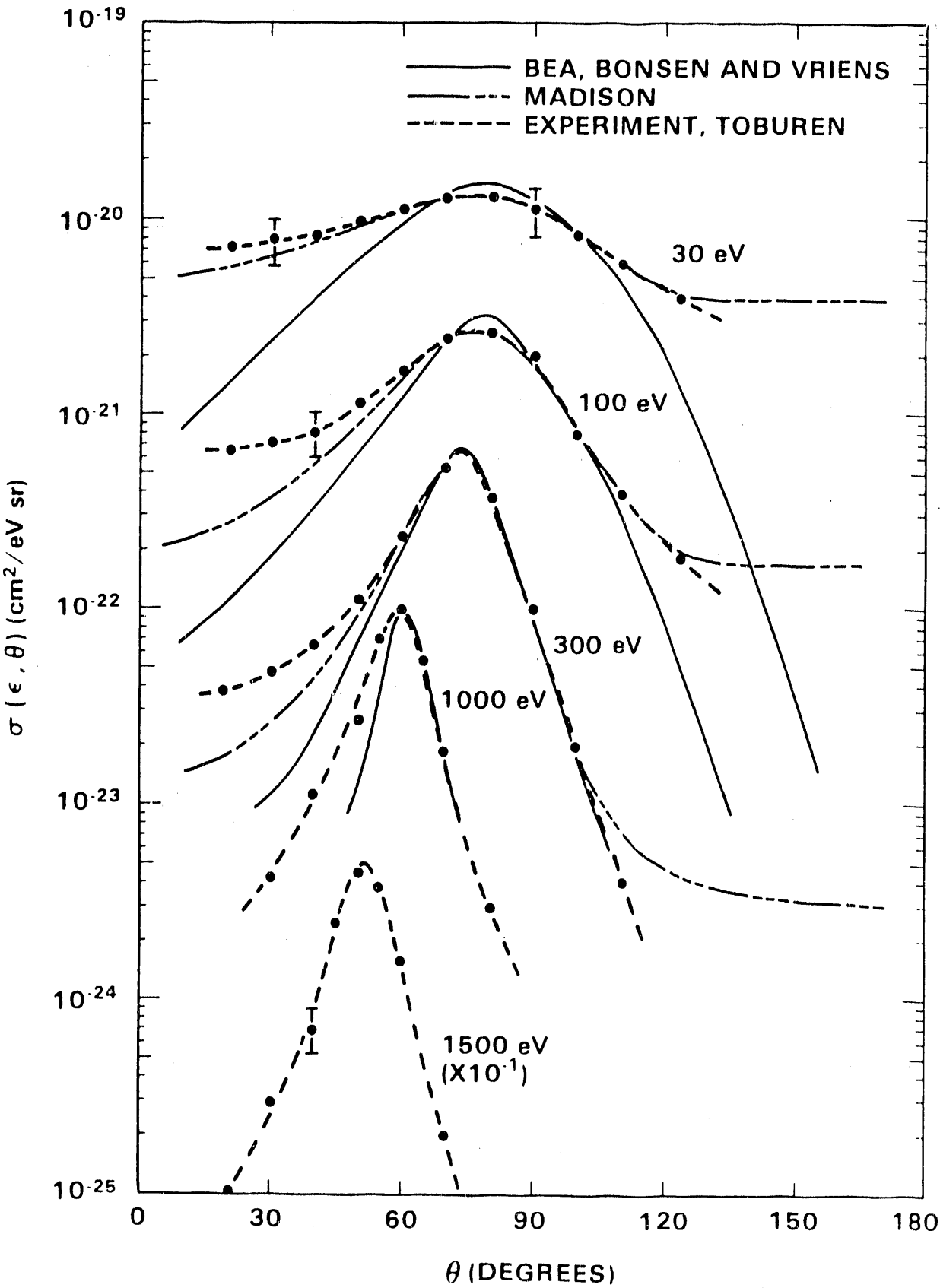

FIGURE 14

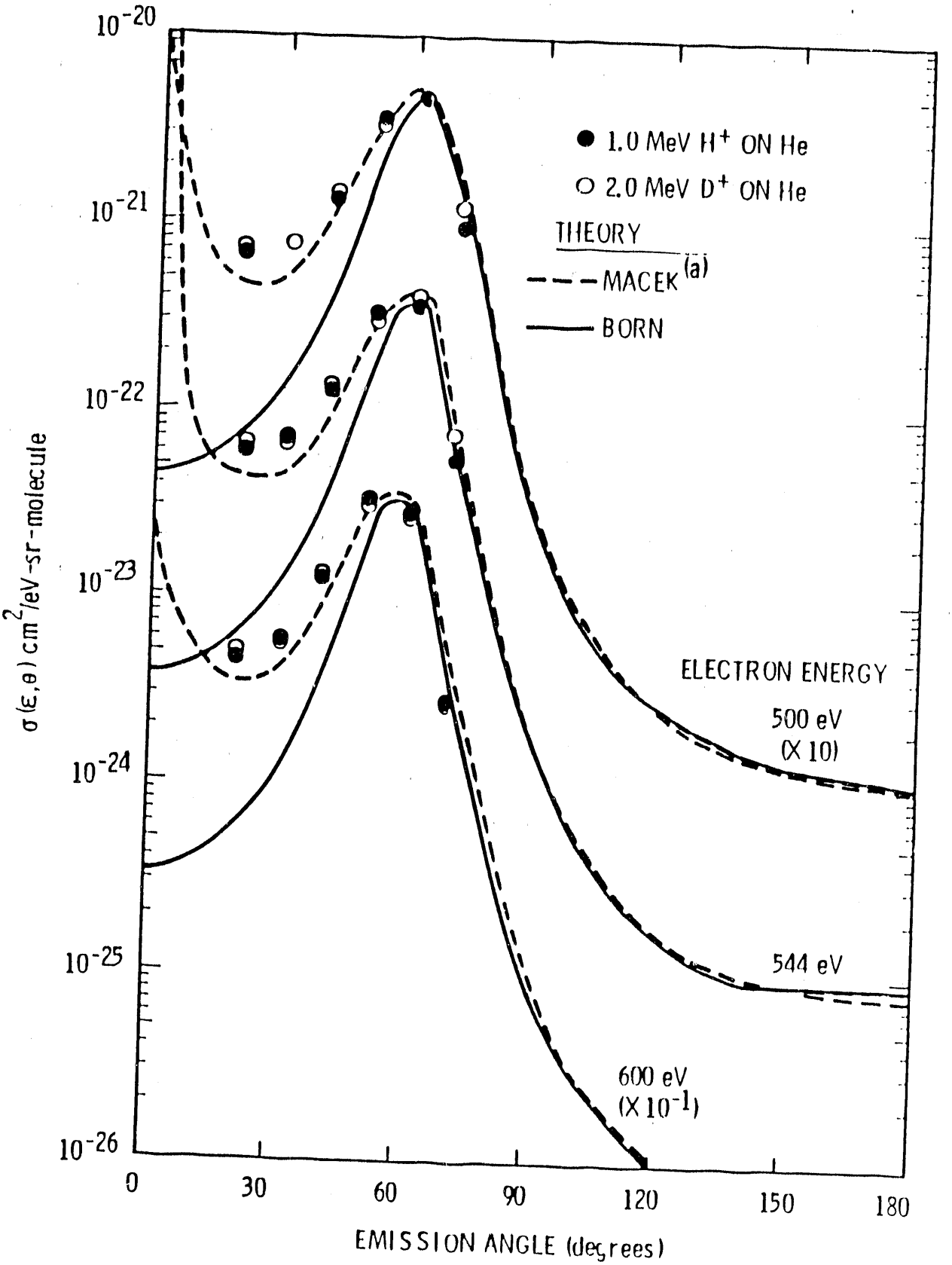
10^{-20}
10^{-21}
10^{-22}
10^{-23}
10^{-24}
10^{-25}
10^{-26}
$\sigma(\epsilon,\theta)$ cm^2/eV-sr-molecule
● 1.0 MeV H^+ ON He
○ 2.0 MeV D^+ ON He
THEORY
MACEK (a)
BORN
ELECTRON ENERGY
500 eV
(X 10)
544 eV
600 eV
(X 10^{-1})
0
30
60
90
120
150
180
EMISSION ANGLE (degrees)

FIGURE 15

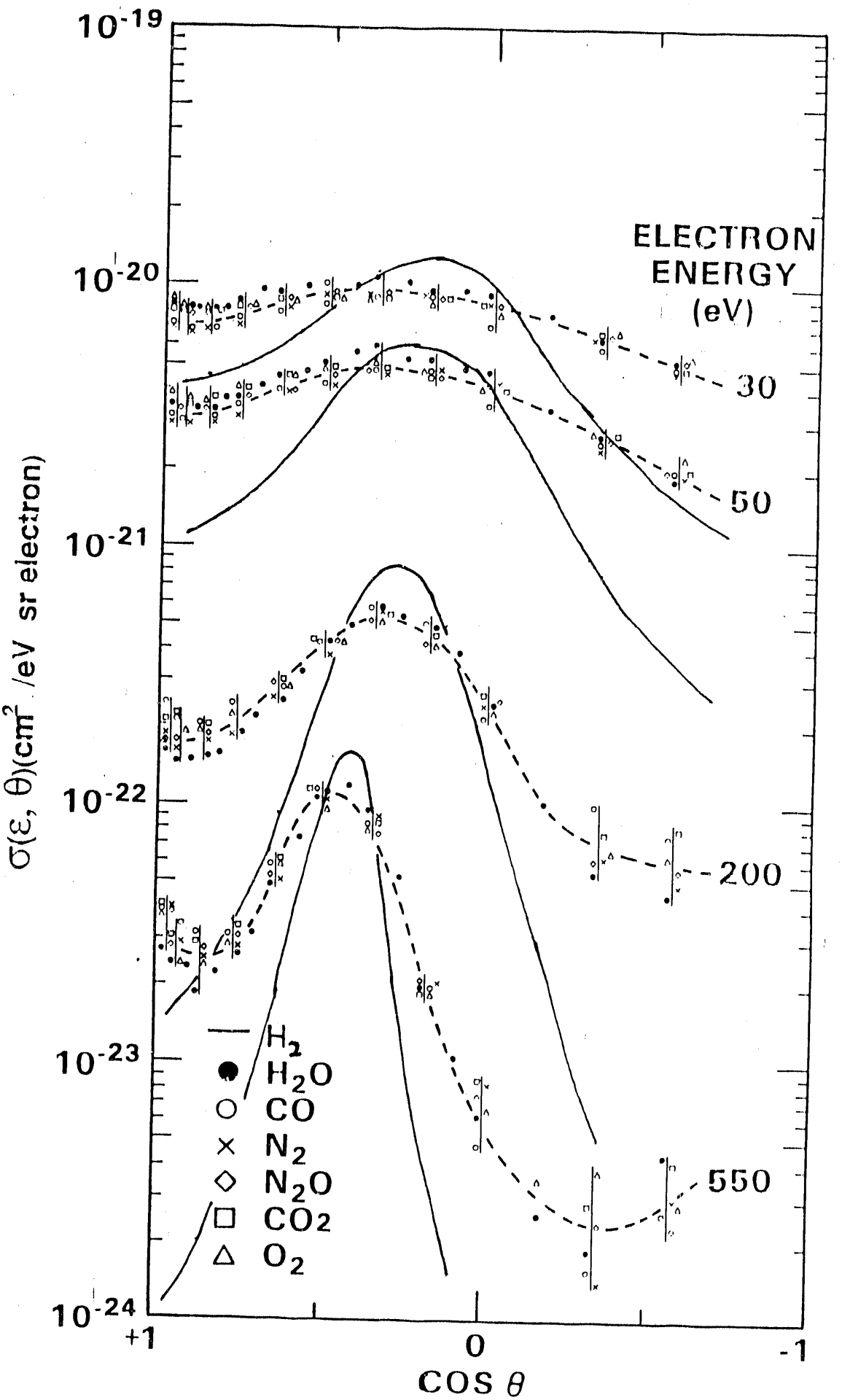
1.5 MeV
10^{-19}
10^{-20}
10^{-21}
10^{-22}
10^{-23}
10^{-24}
$\sigma(\varepsilon, \theta)$(cm^2 /eV sr electron)
ELECTRON ENERGY (eV)
30
50
200
550
H_2
H_2O
CO
N_2
N_2O
CO_2
O_2
+1
0
-1
COS θ

FIGURE 16

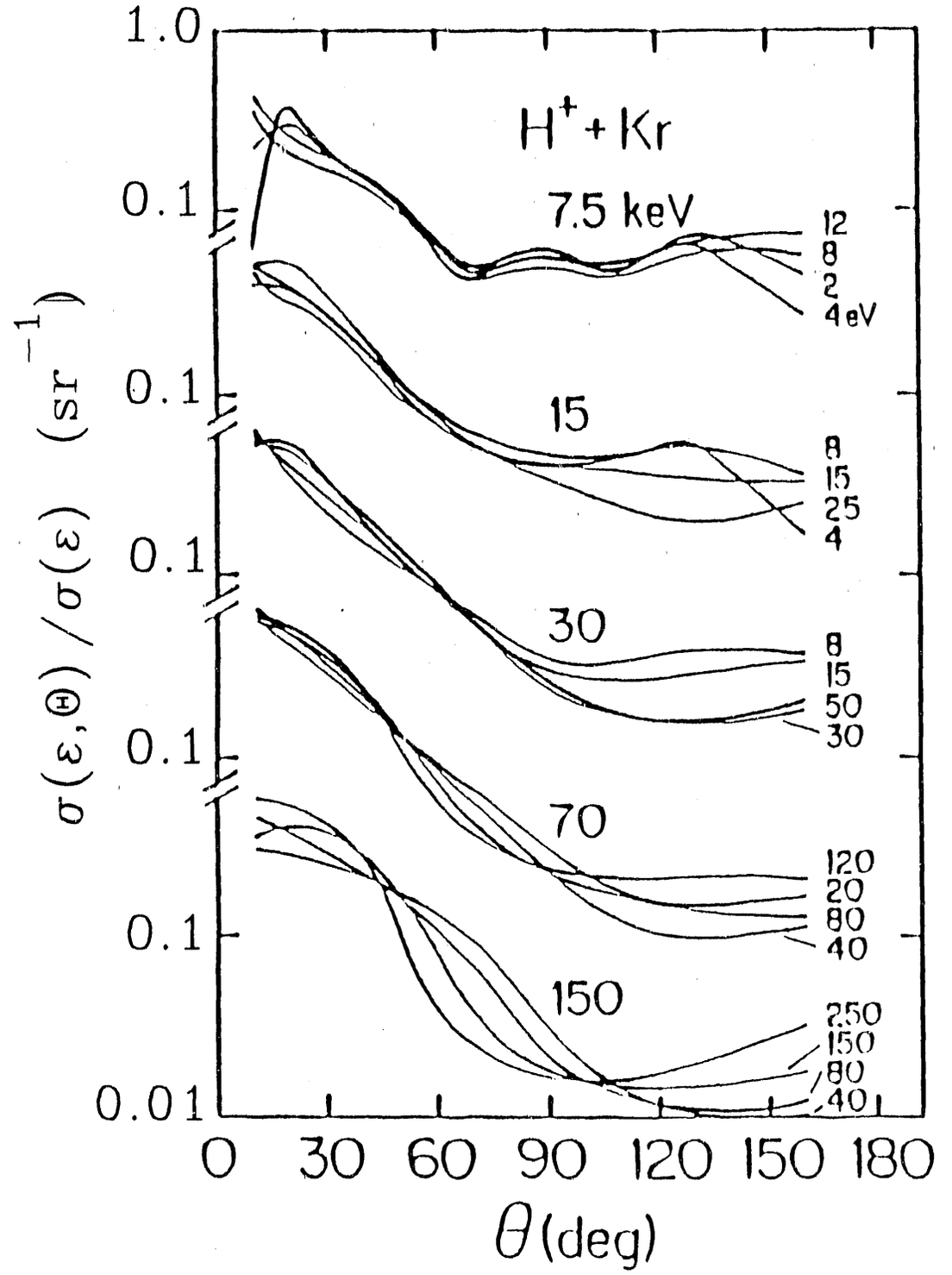
1.0
0.1
0.1
0.1
0.1
0.1
0.01
$H^+ + Kr$
7.5 keV
12
8
2
4 eV
15
8
15
25
4
30
8
15
50
30
70
120
20
80
40
150
250
150
80
40
0
30
60
90
120
150
180
θ(deg)
$\sigma(\omega,\Theta)/\sigma(\omega)$ (sr^{-1})

FIGURE 17

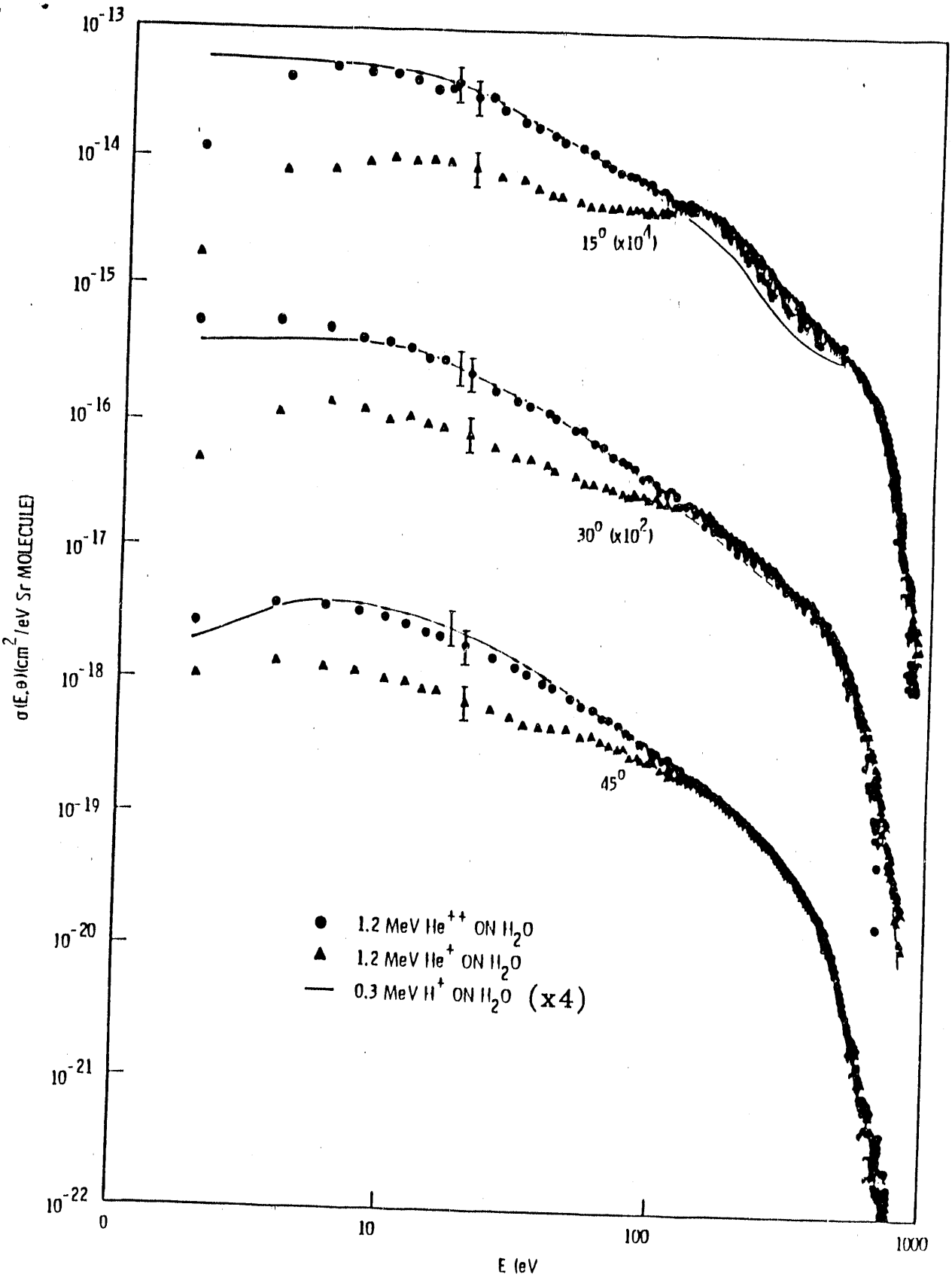
10^{-13}
10^{-14}
10^{-15}
10^{-16}
10^{-17}
10^{-18}
10^{-19}
10^{-20}
10^{-21}
10^{-22}
$\sigma(E,\theta)$/cm^2/eV Sr MOLECULE)
15^0 (x10^1)
30^0 (x10^2)
45^0
1.2 MeV He^{++} ON H_2O
1.2 MeV He^+ ON H_2O
0.3 MeV H^+ ON H_2O (x4)
0
10
100
1000
E (eV

FIGURE 18

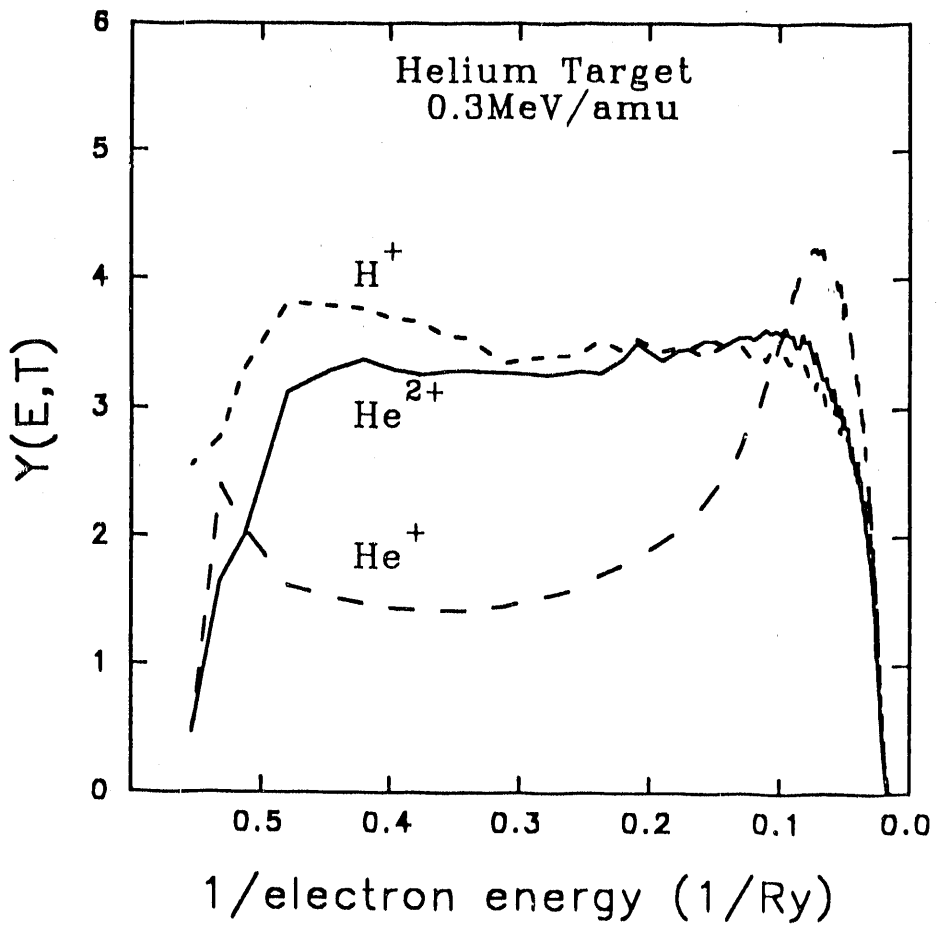
Helium Target
0.3MeV/amu
H+
He2+
He+
Y(E,T)
6
5
4
3
2
1
0
0.5
0.4
0.3
0.2
0.1
0.0
1/electron energy (1/Ry)

FIGURE 19

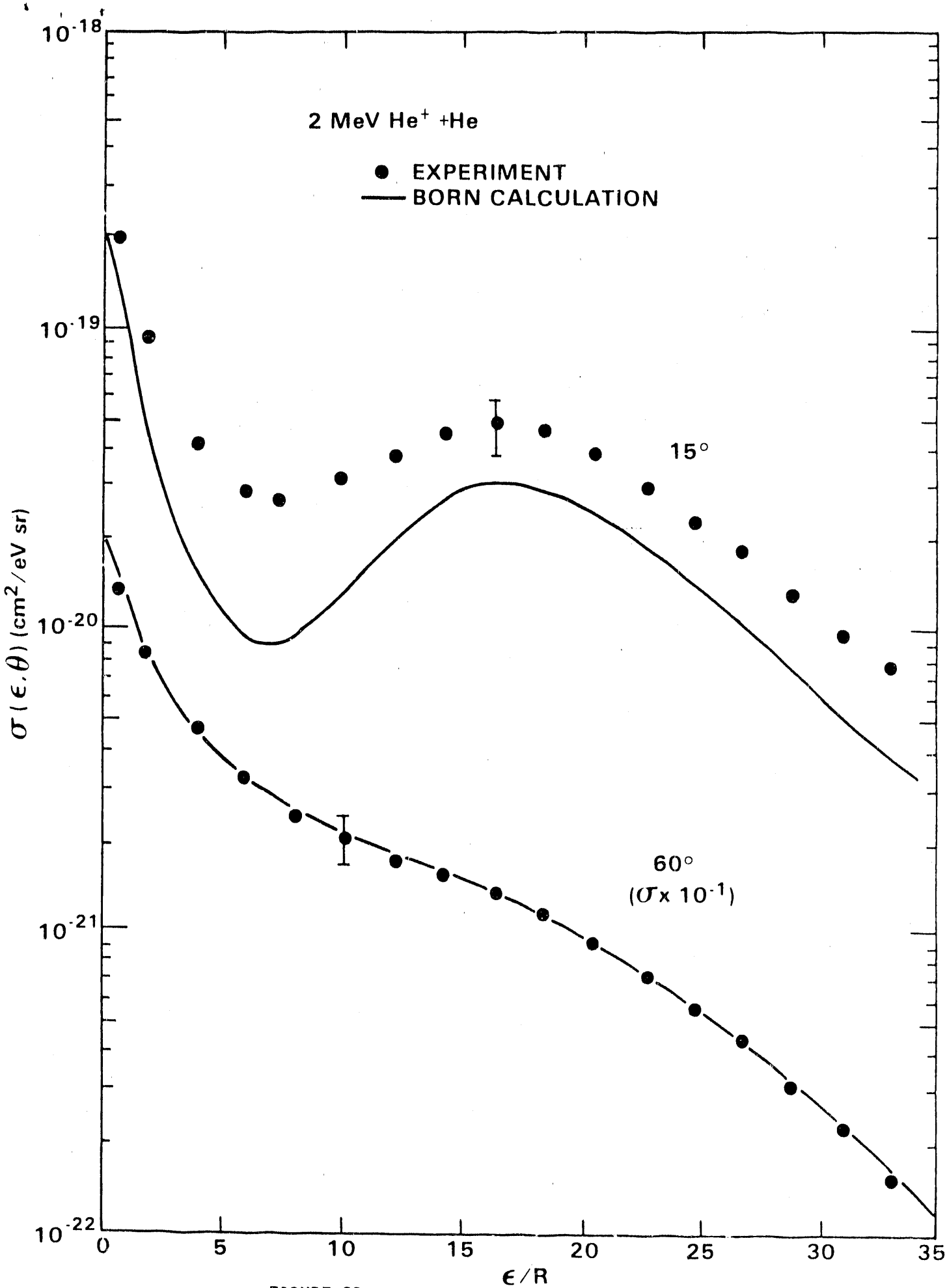
2 MeV He+ +He
EXPERIMENT
BORN CALCULATION
15°
60°
(σx 10-1)
σ(ϵ,θ) (cm2/eV sr)
ϵ/R
10-18
10-19
10-20
10-21
10-22
0
5
10
15
20
25
30
35

FIGURE 20

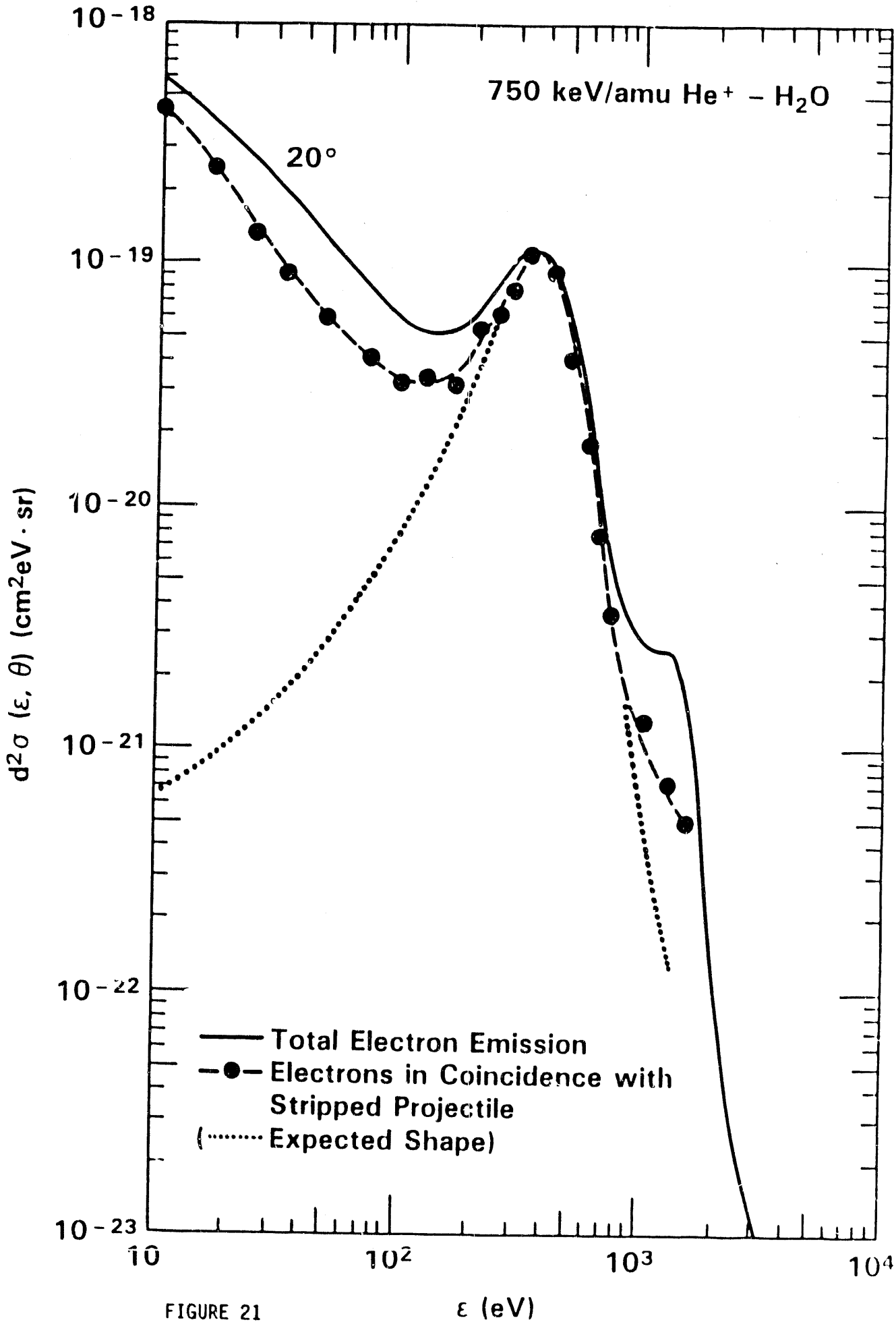
750 keV/amu He+ – H2O
20°
10-18
10-19
10-20
10-21
10-22
10-23
d2σ (ε, θ) (cm2eV · sr)
Total Electron Emission
Electrons in Coincidence with Stripped Projectile
(····· Expected Shape)
10
10²
10³
10⁴
ε (eV)

FIGURE 21

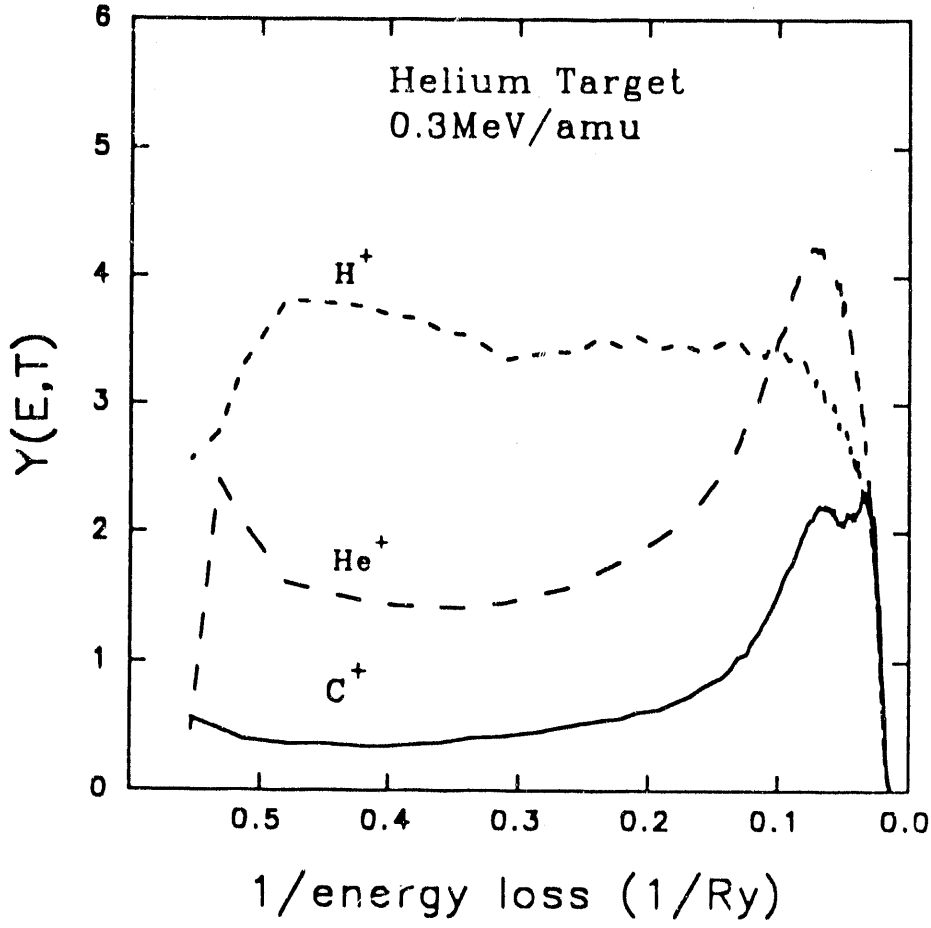
Helium Target
0.3MeV/amu
H+
He+
C+
Y(E,T)
6
5
4
3
2
1
0
0.5
0.4
0.3
0.2
0.1
0.0
1/energy loss (1/Ry)

FIGURE 22

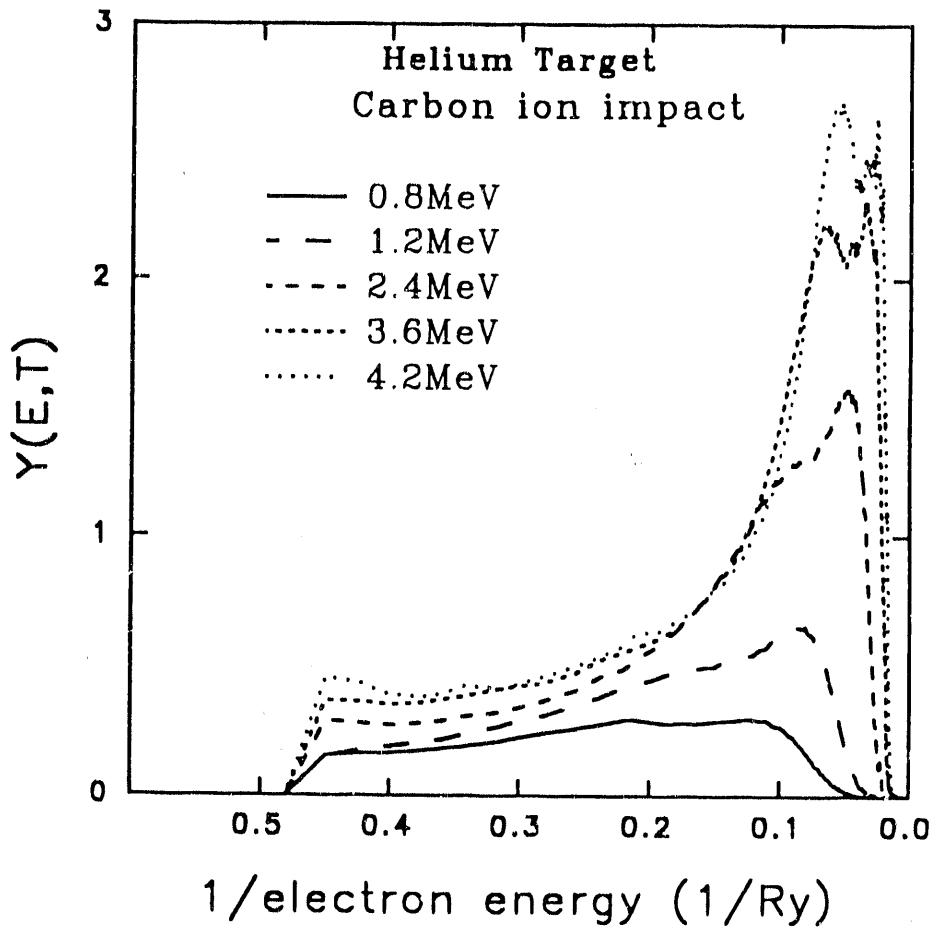
Helium Target
Carbon ion impact
0.8MeV
1.2MeV
2.4MeV
3.6MeV
4.2MeV
Y(E,T)
3
2
1
0
0.5
0.4
0.3
0.2
0.1
0.0
1/electron energy (1/Ry)

FIGURE 23

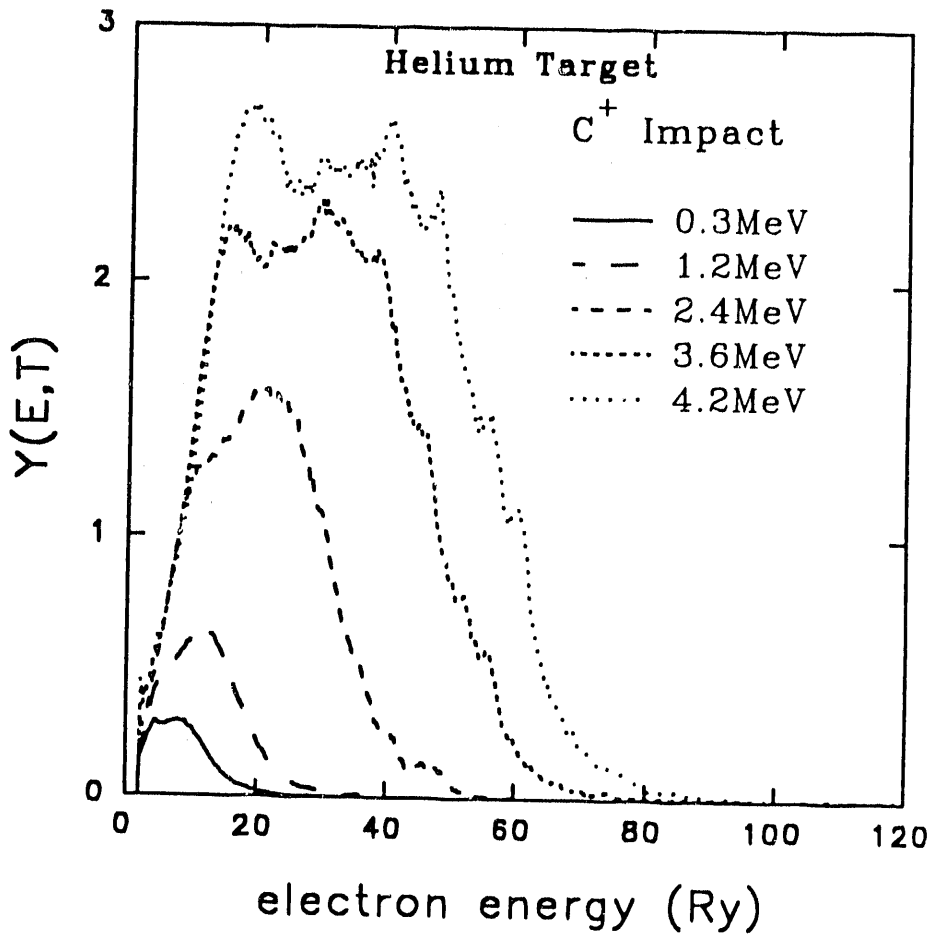
Helium Target
C+ Impact
0.3MeV
1.2MeV
2.4MeV
3.6MeV
4.2MeV
Y(E,T)
electron energy (Ry)
0
1
2
3
0
20
40
60
80
100
120

FIGURE 24

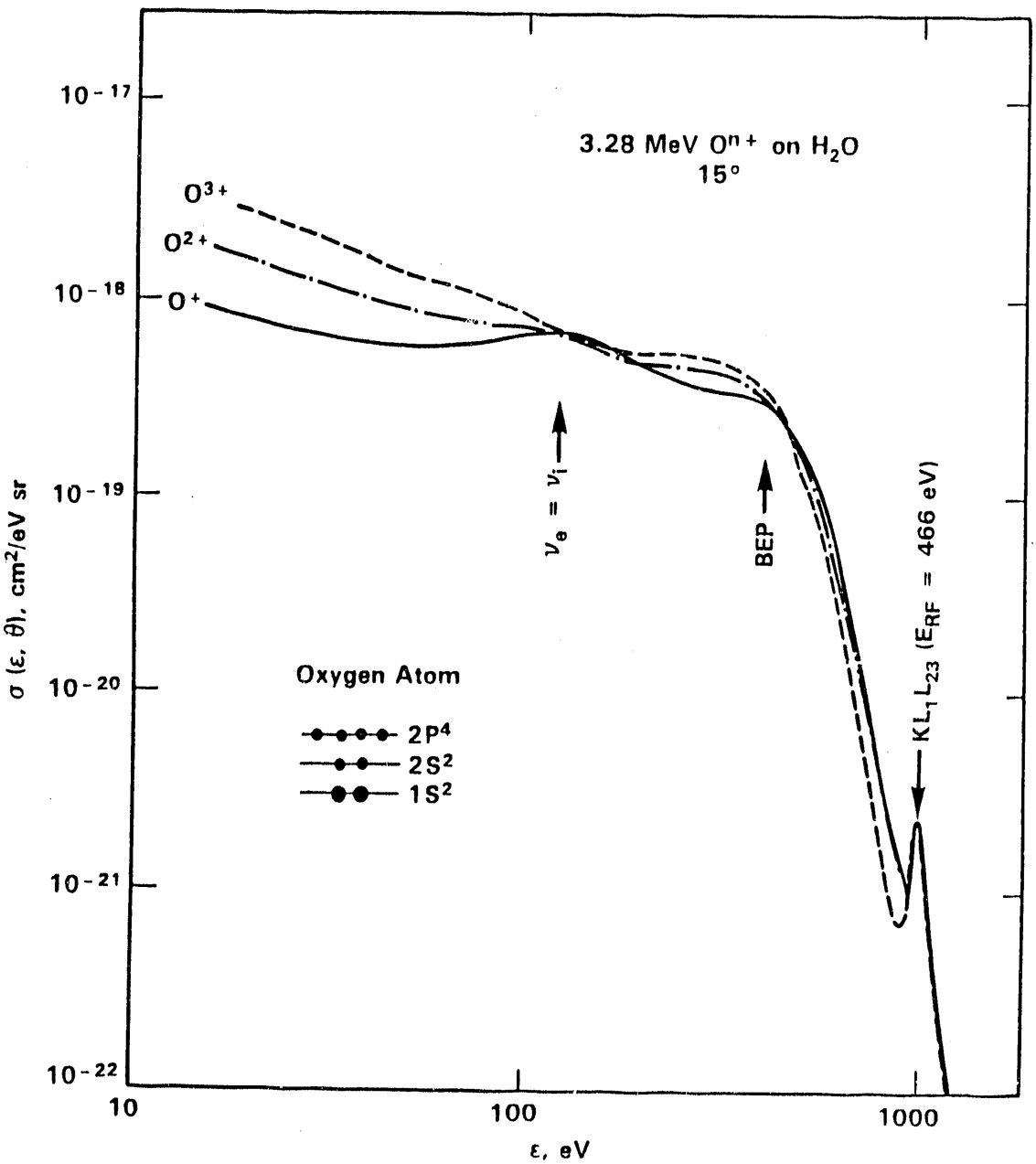
3.28 MeV O^{n+} on H_2O
15°
O^{3+}
O^{2+}
O^{+}
$v_e = v_1$
BEP
KL_1L_{23} (E_{RF} = 466 eV)
Oxygen Atom
$2P^4$
$2S^2$
$1S^2$
σ (ε, θ), cm²/eV sr
10^{-17}
10^{-18}
10^{-19}
10^{-20}
10^{-21}
10^{-22}
10
100
1000
ε, eV

FIGURE 25

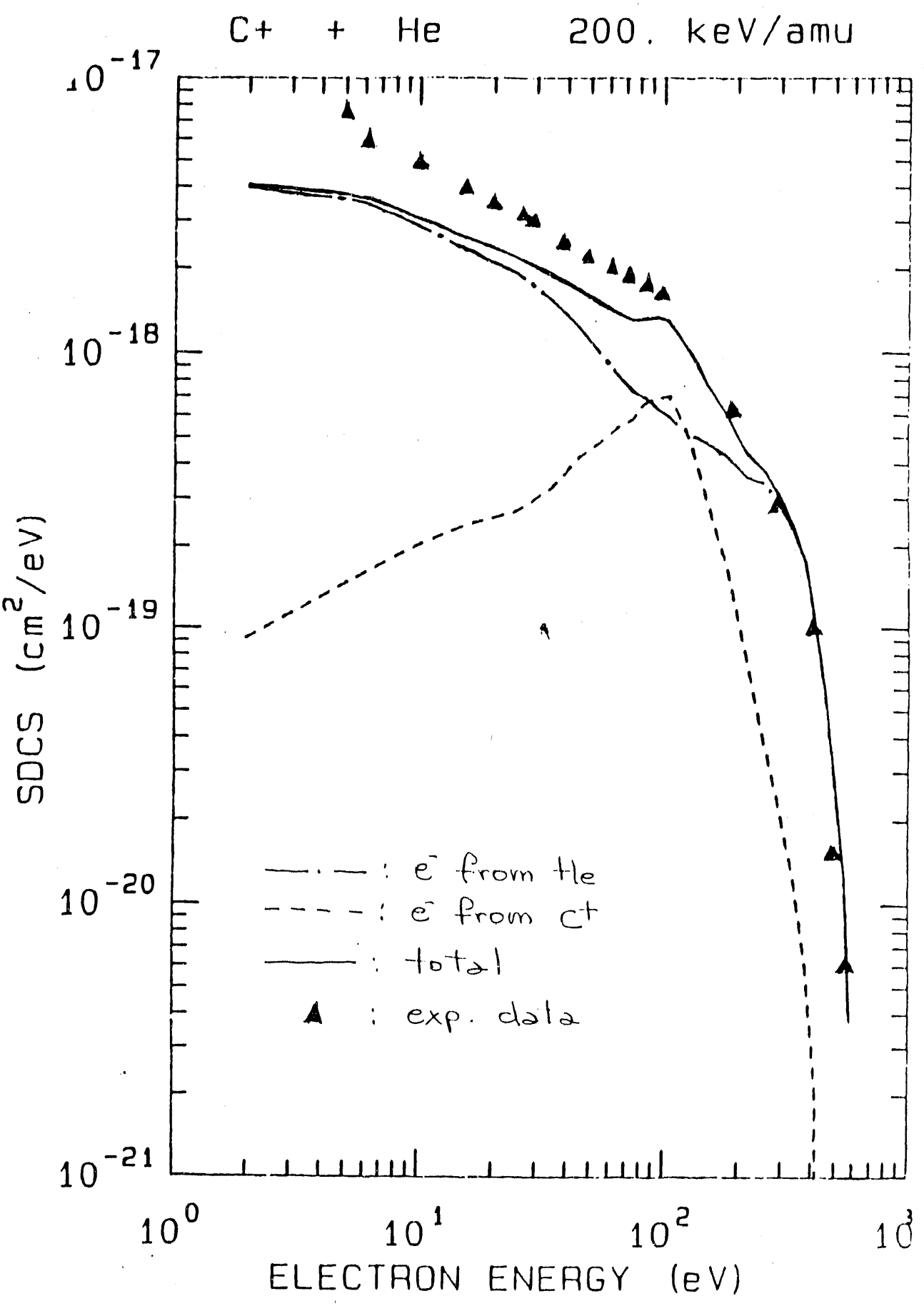
C+ + He 200. keV/amu
SDCS (cm²/eV)
10⁻¹⁷
10⁻¹⁸
10⁻¹⁹
10⁻²⁰
10⁻²¹
10⁰
10¹
10²
ELECTRON ENERGY (eV)
—·— : e⁻ from He
- - - - : e⁻ from C⁺
——— : total
▲ : exp. data

FIGURE 26

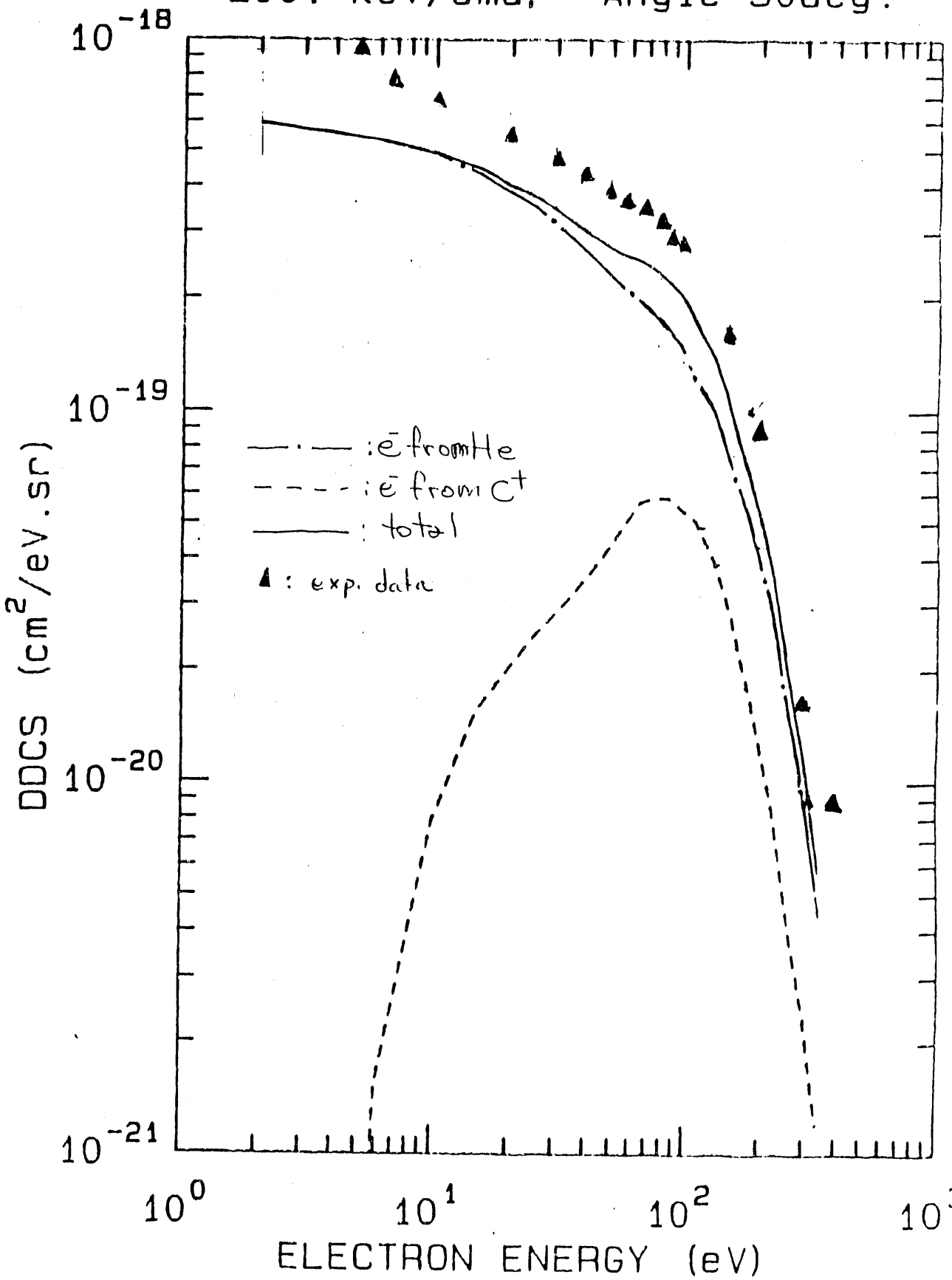
200. keV/amu, Angle=50deg.
10^{-18}
10^{-19}
10^{-20}
10^{-21}
DDCS (cm^2/eV.sr)
: $\bar{e}$ from He
: $\bar{e}$ from C^+
: total
▲ : exp. data
10^0
10^1
10^2
10^3
ELECTRON ENERGY (eV)

FIGURE 27

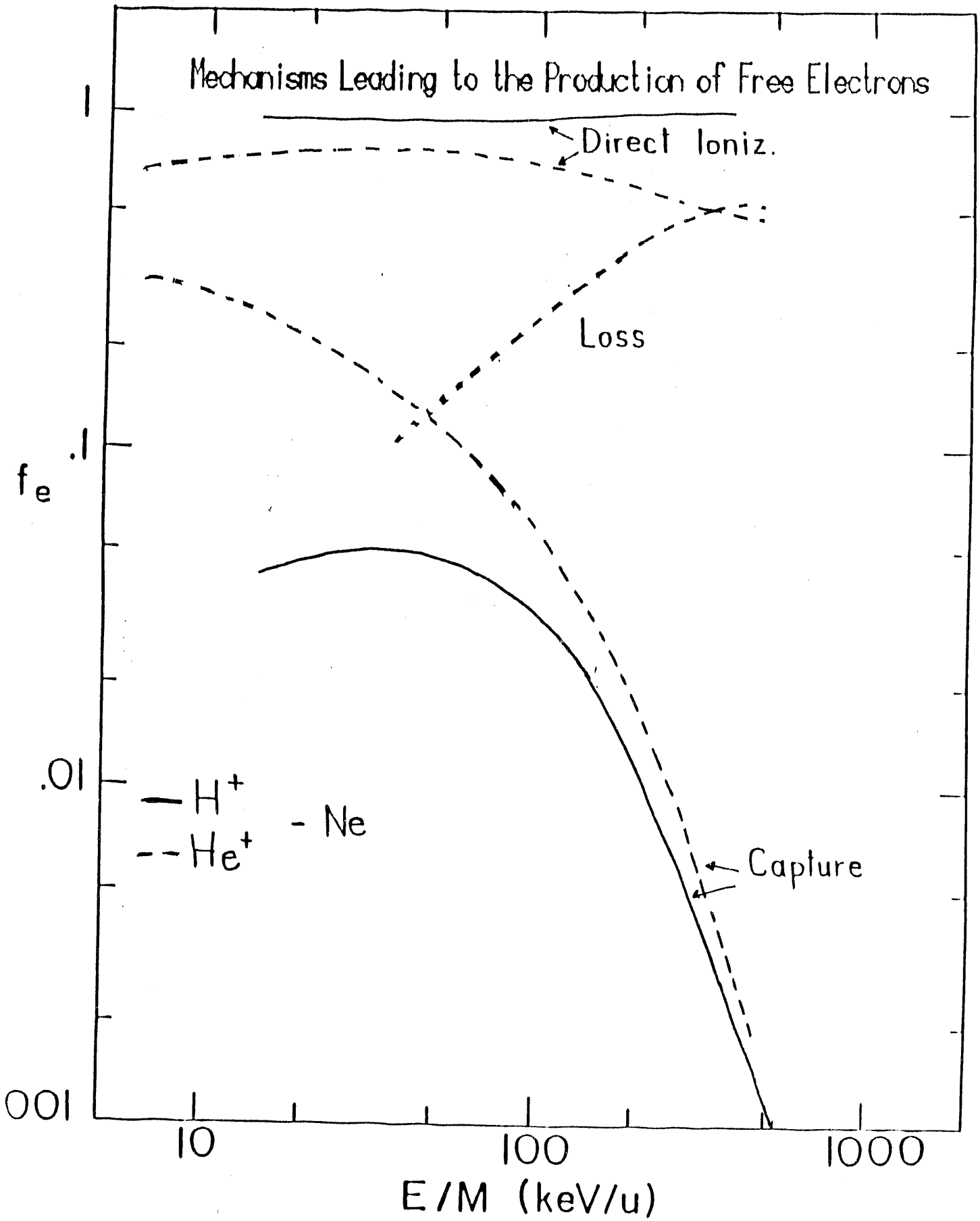
Mechanisms Leading to the Production of Free Electrons
Direct Ioniz.
Loss
Capture
H^+
He^+
- Ne
f_e
1
.1
.01
001
10
100
1000
E/M (keV/u)

FIGURE 28

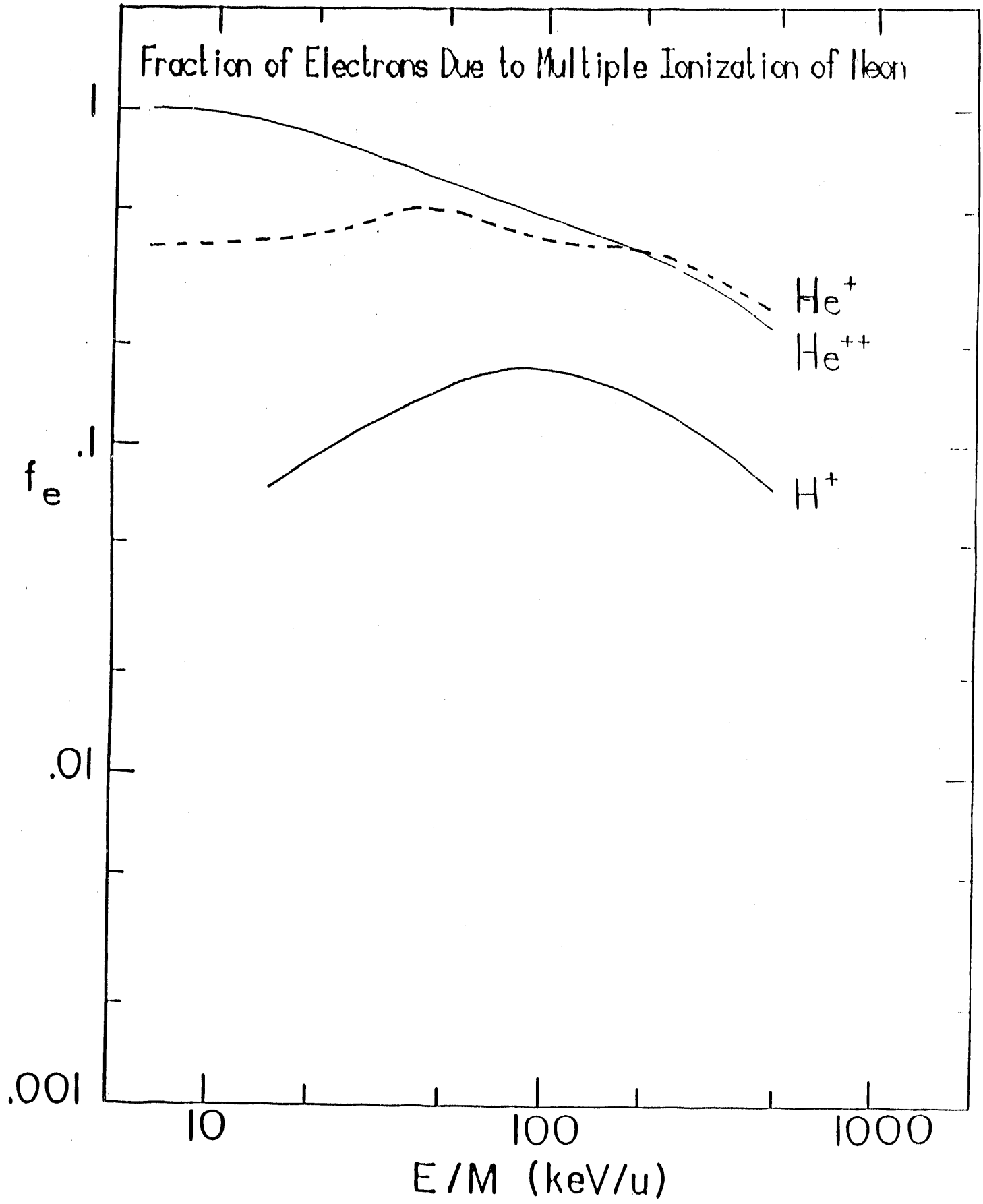
Fraction of Electrons Due to Multiple Ionization of Neon
1
.1
.01
.001
f_e
He^+
He^{++}
H^+
10
100
1000
E/M (keV/u)

FIGURE 29

APPENDIX

TABLE I

PUBLISHED DOUBLE DIFFERENTIAL CROSS SECTIONS

ELECTRON IMPACT

Target	Ion Energy Range (keV)	Ejected Electron Energy (eV)	Ejected Electron Angle (Degrees)	Investigators
He	500 - 300	$1-1/2(E_p-I)$	6 - 156	Shyn and Sharp (1979a)
He	100, 200	$3-(E_p-I)$	10 - 150	Rudd and DuBois (1977)
He	50 - 2000	4 - 2000	30 - 150	Opal, Beaty, and Peterson (1971, 1972)
He	200 - 2000	$2 - E_p$	30 - 150	Goruganthu and Bonham (1986)
He	500, 1000	25 - 45	10 - 130	Oda, Nishimura, and Tahira (1972)
Ne	100 - 500	$4-(E_p-I)$	10 - 150	DuBois and Rudd (1978)
Ne	500	4 - 200	30 - 150	Opal, Beaty, and Peterson (1971, 1972)
Ar	100 - 500	$4-(E_p-I)$	10 - 150	DuBois and Rudd (1978)
Ar	500	4 - 200	30 - 150	Opal, Beaty, and Peterson (1971, 1972)
Ar	1000	4 - 500	90	Mathis and Vroom (1976)
Kr	500	4 - 200	30 - 150	Opal, Beaty, and Peterson (1971, 1972)
Kr	1000	21 - 52	10 - 130	Oda, Nishimura, and Tahira (1972)
Xe	500	4 - 200	30 - 150	Opal, Beaty, and Peterson (1971, 1972)
H_2	100 - 500	$4-(E_p-I)$	10 - 150	DuBois and Rudd (1978)
H_2	500	4 - 200	30 - 150	Opal, Beaty, and Peterson (1971, 1972)

TABLE I (contd)

PUBLISHED DOUBLE DIFFERENTIAL CROSS SECTIONS

ELECTRON IMPACT

Target	Ion Energy Range (keV)	Ejected Electron Energy (eV)	Ejected Electron Angle (Degrees)	Investigators
H_2	25 - 250	$1\text{-}1/2(E_p\text{-}I)$	12 - 156	Shyn, Sharp, and Kim (1981)
N_2	100 - 500	$4\text{-}(E_p\text{-}I)$	10 - 150	DuBois and Rudd (1978)
N_2	50 - 2000	4 - 200	30 - 150	Opal, Beaty, and Peterson (1971, 1972)
N_2	200 - 2000	$2\text{-}E_p$	30 - 150	Goruganthu, Wilson, and Bonham (1987)
N_2	1000	4 - 500	90	Mathis and Vroom (1976)
N_2	50 - 400	$1\text{-}1/2(E_p\text{-}I)$	12 - 156	Shyn (1983)
O_2	50 -2000	4 - 200	30 - 150	Opal, Beaty, and Peterson (1971, 1972)
CH_4	200	4 - 200	30 - 150	Opal, Beaty, and Peterson (1971, 1972)
CH_4	500, 1000	5 - 1000	15 - 148	Oda (1975)
NH_3	200	4 - 200	30 - 150	Opal, Beaty, and Peterson (1971, 1972)
H_2O	50 - 2000	$2\text{-}(E_p\text{-}I_p)$	15 - 150	Bolorizadeh and Rudd (1986a)
H_2O	500	4 - 200	30 - 150	Opal, Beaty, and Peterson (1971, 1972)
H_2O	1000	4 - 500	90	Mathis and Vroom (1976)
H_2O (clusters)	1000	4 - 500	90	Mathis and Vroom (1976)
H_2O	500, 1000	5 - 1000	15 - 148	Oda (1975)

TABLE I (contd)

PUBLISHED DOUBLE DIFFERENTIAL CROSS SECTIONS

ELECTRON IMPACT

Target	Ion Energy Range (keV)	Ejected Electron Energy (eV)	Ejected Electron Angle (Degrees)	Investigators
C_2H_2	500	4 - 200	30 - 150	Opal, Beaty, and Peterson (1971, 1972)
CO	800	.9 - 393	30 - 150	Ma and Bonham (1988)
CO	500	4 - 200	30 - 150	Opal, Beaty, and Peterson (1971, 1972)
NO	500	4 - 200	30 - 150	Opal, Beaty, and Peterson (1971, 1972)
CO_2	500	4 - 200	30 - 150	Opal, Beaty, and Peterson (1971, 1972)
CO_2	50 - 400	$1-1/2(E_p-I)$	12 - 156	Shyn and Sharp (1979b)
CO_2	500, 1000	5 - 1000	15 - 148	Oda (1975)

TABLE II

PUBLISHED DOUBLE DIFFERENTIAL CROSS SECTIONS

PROTON IMPACT

Target	Ion Energy Range (keV)	Ejected Electron Energy (eV)	Ejected Electron Angle (Degrees)	Investigators
H_2	50 - 100	4 - 300	23 - 152	Kuyatt and Jorgensen (1963)
H_2	50 - 100	1 - 500	10 - 160	Rudd and Jorgensen (1963)
H_2	100 - 300	2 - 1000	10 - 160	Rudd, Sautter and Bailey (1966)
H_2	300	2 - 800	20 - 130	Toburen (1971a)
H_2	300 - 1500	2 - 3500	20 - 130	Toburen and Wilson (1972)
H_2	1000	100 - 1000	20 - 130	Toburen (1971b)
H_2	5 - 100	1.5 - 300	10 - 160	Rudd (1979)
He	75 - 150	1 - 550	10 - 160	Cheng, Rudd, and Hsu (1989)
He	50 - 150	1 - 500	10 - 160	Rudd and Jorgensen (1963)
He	100 - 300	2 - 1000	10 - 160	Rudd, Sautter, and Bailey (1966)
He	2 - 100	5 - 100	0 - 100	Gibson and Reid (1986)
He	2000	30 - 1500	20 - 130	Toburen (1971b)
He	300	1 - 1030	20 - 150	Stolterfoht (1971a)
He	300 - 5000	1 - 8577	15 - 160	Manson, Toburen, Madison and Stolterfoht (1975)
He	5 - 5000	1 - 8577	10 - 160	Rudd, Toburen and Stolterfoht (1976)
He	5 - 100	10 - 200	10 - 160	Rudd, Webster, Blocker, and Madison (1975)
He	300 - 1500	1 - 3500	15 - 125	Toburen, Manson, and Kim (1978)
He	5 - 100	10 - 200	10 - 160	Rudd and Madison (1976)
He	100 - 300	40 - 180	0	Crooks and Rudd (1970)

TABLE II (cont'd)

PUBLISHED DOUBLE DIFFERENTIAL CROSS SECTIONS

PROTON IMPACT

Target	Ion Energy Range (keV)	Ejected Electron Energy (eV)	Ejected Electron Angle (Degrees)	Investigators
Ne	7.5 - 150	1 - 550	10 - 160	Cheng, Rudd, and Hsu (1989)
Ne	50 - 300	1.5 - 1057	10 - 160	Crooks and Rudd (1971)
Ne	1000	1 - 2000	15 - 125	Toburen and Manson (1973)
Ne	300 - 1500	1 - 3500	15 - 125	Toburen, Manson, and Kim (1978)
Ar	50 - 300	1.5 - 1057	10 - 160	Crooks and Rudd (1971)
Ar	5 - 1500	1 - 3500	15 - 160	Criswell, Toburen, and Rudd (1971)
Ar	300 - 5000	1.1 - 10000	25 - 150	Gabler (1974)
Ar	5 - 2000	1 - 3500	15 - 125	Criswell, Wilson, and Toburen (1975)
Ar	1000	1 - 360	15 - 125	Manson and Toburen (1975)
Ar	300 - 1500	1 - 3500	15 - 125	Toburen, Manson, and Kim (1978)
Ar	100	3 - 250	160	Rudd, Jorgensen, and Volz (1966)
Ar	5 - 20	1 - 26	30 - 140	Sataka, Okuno, Urakawa and Oda (1979)
Ar	5 - 5000	1 - 10000	10 - 160	Rudd, Toburen, and Stolterfoht (1979)
Kr	7.5 - 150	1 - 550	10 - 1601	Cheng, Rudd, and Hsu (1989)
Kr	1000	1 - 3000	15 & 90	Manson and Toburen (1977)
Kr	1000 - 4200	30, 136	15 - 90	Toburen and Manson (1979)
Xe	300 - 2000	2 - 4620	20 - 130	Toburen (1974)
N_2	300 - 1700	2 - 4000	20 - 130	Toburen (1971a)

TABLE II (cont'd)

PUBLISHED DOUBLE DIFFERENTIAL CROSS SECTIONS

PROTON IMPACT

Target	Ion Energy Range (keV)	Ejected Electron Energy (eV)	Ejected Electron Angle (Degrees)	Investigators
N_2	50 - 300	1.5 - 1057	10 - 160	Crooks and Rudd (1971)
N_2	200 - 500	1 - 1300	20 - 150	Stolterfoht (1971a)
N_2	5 - 70	1.5 - 300	10 - 160	Rudd (1979)
N_2	200 - 500	1 - 1300	20 - 150	Stolterfoht (1971b)
O_2	50 - 300	1.5 - 1057	10 - 160	Crooks and Rudd (1971)
O_2	300 - 1500	1 - 3500	15 - 125	Toburen and Wilson (1977a)
H_2O	15 - 150	1 - 3000	10 - 160	Bolorizadeh and Rudd (1986b)
H_2O	300 - 1500	1 - 3500	15 - 125	Toburen and Wilson (1977a)
CH_4	200 - 400	1 - 1270	20 - 150	Stolterfoht (1971a)
CH_4	300 - 1000	4 - 5000	20 - 130	Wilson and Toburen (1975)
CH_4	250 - 2000	1 - 5000	20 - 130	Lynch, Toburen, and Wilson)1976)
C_2H_2	300 - 1000	4 - 5000	20 - 130	Wilson and Toburen (1975)
C_2H_4	300 - 1000	4 - 5000	20 - 130	Wilson and Toburen (1975)
C_2H_6	300 - 1000	4 - 5000	20 - 130	Wilson and Toburen (1975)
C_6H_6	300 - 2000	4 - 5000	20 - 130	Wilson and Toburen (1975)
NH_3	25 - 2000	1 - 5000	20 - 130	Lynch, Toburen, and Wilson (1976)
CH_3NH_2	250 - 2000	1 - 5000	20 - 130	Lynch, Toburen, and Wilson (1976)
$(CH_3)_2NH$	250 - 2000	1 - 5000	20 - 130	Lynch, Toburen, and Wilson (1976)

TABLE II (cont'd)

PUBLISHED DOUBLE DIFFERENTIAL CROSS SECTIONS

PROTON IMPACT

Target	Ion Energy Range (keV)	Ejected Electron Energy (eV)	Ejected Electron Angle (Degrees)	Investigators
TeF_6	300 - 1800	1 - 5000	20 - 130	Toburen, Wilson, and Porter (1977
SF_6	300 - 1800	1 - 5000	20 - 130	Toburen, Wilson, and Porter (1977)

TABLE III

PUBLISHED DOUBLE DIFFERENTIAL CROSS SECTIONS

STRUCTURED-ION IMPACT

Reaction	Ion Energy Range (keV)	Ejected Electron Energy Range (kev)	Ejected Electron Angle (Degrees)	Investigators
$H_2^+ + H_2$	600 - 1500	2 - 2000	20 - 125	Wilson and Toburen (1973)
$Ne^+ + Ne$	50 - 300	1.5 - 1000	10 - 160	Cacak and Jorgensen (1970)
$Ne^{n+} + Ne$ (n=1-4)	25 - 800	1.6 - 1100	45 - 135	Woerlee, Gordeev, de Waard, and Saris (1981)
$Ar^+ + Ar$	50 - 300	1.5 - 1000	10 - 160	Cacak and Jorgensen (1970)
$Ar^+ + Ar$	100	3 - 250	160	Rudd, Jorgensen, and Volz (1966)
$O^{n+} = O_2$ (n=4-8)	30000	10 - 4000	25 - 90	Stolterfoht, et al. (1974)
$\left.\begin{matrix} H_2^+ \\ He^+ \end{matrix}\right\} + \left\{\begin{matrix} H_2 \\ He \end{matrix}\right.$	1000, 2000	20 - 1000	30 - 140	Oda and Nishimura (1979)
$\left.\begin{matrix} H_2^+ \\ He^o \end{matrix}\right\} + Ar$	5 - 20	1 - 26	30 - 140	Sataka, Okuno, Urakawa, and Oda (1979)
$\left.\begin{matrix} H^o + He \\ H_2^o + He \\ {}^3He^o + He \\ {}^4He^o + He \end{matrix}\right\}$	15 - 150	1.5 - 300	10 - 160	Fryar, Rudd, and Risley (1977)
$H^o = He$	15 - 150	1.5 - 300	15 - 150	Rudd, Risley, Friar, and Rolfes (1980)

TABLE III (contd)

PUBLISHED DOUBLE DIFFERENTIAL CROSS SECTIONS

STRUCTURED-ION IMPACT

Reaction	Ion Energy Range (keV)	Ejected Electron Energy Range (kev)	Ejected Electron Angle (Degrees)	Investigators
He^+, He^{++} + He, Ne, Ar	1200	1 - 3500	15 - 125	Toburen and Wilson (1977b)
He^+, He^{++} + Ar	300 - 2000	1 - 4000	15 - 125	Toburen and Wilson (1979)
He^+, He^{2+} + H_2O	300 - 2000	1 - 4000	15 - 125	Toburen, Wilson, and Popowich (1980)
H^o + H_2O	20 - 150	1 - 300	10 - 160	Bolorizadeh and Rudd (1986c)
H_2^+, H_3^+ + He	5 - 20	2 - 50	30 - 120	Urakawa, Tokoro, and Oda (1981)
H^+, H_2^+, He^+ + Ar	5 - 20	2 - 26	30, 90	Sataka, Urakawa, and Oda (1979)
C^+ + He, Ne, Ar, CH_4	1200	1 - 800	30, 90	Toburen (1979a)
C^+ + He	800 - 4200	10 - 1500	15 - 130	Reinhold, Schultz, Olson, Toburen, and DuBois (In Press) (1990)

TABLE III (contd)

PUBLISHED DOUBLE DIFFERENTIAL CROSS SECTIONS

STRUCTURED-ION IMPACT

Reaction	Ion Energy Range (keV)	Ejected Electron Energy Range (kev)	Ejected Electron Angle (Degrees)	Investigators
C^{+n} + Ar (n=1-3)	1300 - 3000	1 - 4000	15 - 130	Toburen (1979b)
O^+, N^+ } Ar	50 - 500	5 - 500	16 - 160	Stolterfoht and Schneider (1979)
Kr^{n+} + Kr (n=2-5)	50 - 1000	80 - 1000	45 - 135	Gordeev, Woerlee, de Waard, and Saris (1979)
Kr^{n+} + Kr (n=2-5)	25 - 800	16 - 1100	45 - 135	Gordeev, Woerlee, De Waard, and Saris (1981)
H^+, H_2^+, He^+ } + Ar	5 - 20 keV	2 - 26	30 and 90	Sataka, Urakawa, and Oda (1979)
U^{38+} } He; Th^{38+} } Ar	6000/amu	5 - 5000	20 - 150	Schneider et al. (1989)
Mo^{44+} - He	2500/amu	2 - 5000	20 - 160	Stolterfoht et al. (1987)
U^{33+} - Ne	1400/amu	1 - 4000	20-90	Kelbch, Olson, Schmidt, Schmidt-Böcking, and Hagmann (1989)
U^{33+} - Ar	1400/amu	1 - 4000	20 - 90	Kelbch, Olson, Schmidt, Schmidt-Böcking, and Hagmann (1989)

REFERENCES TO TABLES I, II, AND III

M. A. Bolorizadeh and M. E. Rudd, Angular and Energy Dependence of Cross Sections for Ejection of Electrons from Water Vapor. I. 50-2000 eV Electron Impact, *Phys. Rev A* 33: 882-887 (1987a).

M. A. Bolorizadeh and M. E. Rudd, Angular and Energy Dependence of Cross Sections for Ejection of Electrons from Water Vapor. II. 15-150 keV Proton Impact, *Phys. Rev. A* 33: 888-896 (1986b).

M. A. Bolorizadeh and M. E. Rudd, Angular and Energy Dependence of Cross Sections for Ejection of Electrons from Water Vapor. III. 20-150 keV Neutral Hydrogen Impact, *Phys. Rev A* 33: 893-896 (1986c).

R. K. Cacak, and T. Jorgensen, Jr., Absolute Doubly Differential Cross Sections for Production of Electrons in He^+-Ne and Ar^+-Ar Collisions, *Phys. Rev. A* 2: 1322-1327 (1970).

Wen-qin Cheng, M. E. Rudd, and Ying-Yuan Hsu, Differential Cross Sections for Ejection of Electrons from Rare Gases by 7.5-150 keV Protons, *Phys. Rev. A* 39: 2359-2366 (1989).

T. L. Criswell, L. H. Toburen, and M. E. Rudd, Energy and Angular Distributions of Electrons Ejected from Argon by 5 keV to 1.5 MeV Protons, *Phys. Rev. A* 16: 508-517 (1977).

T. L. Criswell, W. E. Wilson, and L. H. Toburen, Energy and Angular Distribution of Electrons Ejected from Argon by 5-2000 keV H_2^+ Impact, in IX International Conference on the Physics of Electronic and Atomic Collisions, Abstracts of Papers (University of Washington Press, Seattle) pp. 749-750 (1975).

G. B. Crooks and M. E. Rudd, Experimental Evidence for the Mechanism of Charge Transfer to Continuum States, *Phys. Rev. Lett.* 25: 1599-1601 (1970).

J. B. Crooks and M. E. Rudd, Angular and Energy Distributions of Cross Sections for Electron Production by 50-300 keV Proton Impacts on N_2, O_2, Ne, and Ar, *Phys. Rev. A* 3: 1628-1634 (1971).

R. D. DuBois and M. E. Rudd, Absolute Doubly Differential Cross Sections for Ejection of Secondary Electrons from Gases by Electron Impact. II. 100-500 eV Electrons on Neon, Argon, Molecular Hydrogen and Molecular Nitrogen, *Phys. Rev. A* 17: 843-848.

J. Fryar, M. E. Rudd, and J. S. Risley, Doubly Differential Cross Sections for Electron Production by Impact of H^0, H_2^0, H_2^0, $^3He^0$, and $^4He^0$ on Helium, in XI International Conference on the Physics of Electronic and Atomic Collisions, Abstracts of Papers (Commissariat A L'Energie Atomique, Paris) pp. 984-985 (1977); and M. E. Rudd, J. S. Risley, and J. Fryar, Double Differential Cross Sections for Electron Production by Neutral Hydrogen on Helium, *Ibid.*, pp. 986-987 (1977).

H. Gabler, Ph.D. Thesis, Free University, Berlin (1974).

D. K. Gibson and I. D. Reid, Double Differential Cross Sections for Electron Ejection from Helium by Fast Protons, *J. Phys. B* 19: 3265-3276 (1986).

Yu. S. Gordeev, P. H. Woerlee, H. de Waard, and F. W. Saris, Continuous Electron Spectra Produced in Kr^{n+} - Kr Collisions, in XI International Conference on the Physics of Electronic and Atomic Collisions, Abstracts of Papers (The Society for Atomic Collision Research, Japan) pp. 746-747 (1979).

Yu. S. Gordeev, P. H. Woerlee, H. de Waard, and F. W. Saris, The Production of Continuous Electron Spectra in Collisions of Heavy Ions and Atoms. A. Molecular Autoionization, *J. Phys. B* 14: 513-526 (1981).

R. R. Goruganthu and R. A. Bonham, Secondary-Electron-Production Cross Sections for Electron Impact Ionization of Helium, *Phys. Rev. A* 34: 103-126 (1986).

R. R. Goruganthu, W. G. Wilson, and R. A. Bonham, Secondary Electron Production Cross Sections for Electron Impact Ionization of Molecular Nitrogen, *Phys. Rev. A* 35: 540-558 (1987).

C. Kelbch, R. E. Olson, S. Schmidt, H. Schmidt-Böcking, and S. Hagmann, Unexpected Angular Distribution of the δ-Electron Emission in 1.4 MeV/amu U^{33+} - Rare Gas Collisions, *J. Phys. B* 22: 2171-2178 (1989).

C. E. Kuyatt and T. Jorgensen, Jr., Energy and Angular Dependence of the Differential Cross Section for Production of Electrons by 50-100 keV Protons in Hydrogen Gas, *Phys. Rev.* 130: 1444-1455 (1963).

D. J. Lynch, L. H. Toburen, and W. E. Wilson, "Electron Emission from Methane, Ammonia, Monomethylamine and Dimethylamine by 0.25 to 2.0 MeV Protons, *J. Chem. Phys.* 64: 2616-2622 (1976).

Ce Ma and R. A. Bonham, Secondary Electron Production Cross Sections for 800 eV Electron-Impact Ionization of Carbon Monoxide, *Phys. Rev. A* 38: 2160-2162 (9188).

S. T. Manson and L. H. Toburen, Energy and Angular Distribution of Electrons Ejected from Ar by 1-MeV Proton Impact Ionization: Theory and Experiment, in IX International Conference on the Physics of Electronic and Atomic Collisions, Abstracts of Papers (University of Washington Press, Seattle) pp. 751-752 (1975).

S. T. Manson and L. H. Toburen, Energy and Angular Distribution of Electrons Ejected from Kr by 1 MeV Proton Impact Ionization: Theory and Experiment, in X International Conference on the Physics of Electronic and Atomic Collisions, Abstracts of Papers (Commissariat A L'Energie Atomique, Paris) pp. 990-991 (1977).

S. T. Manson, L. H. Toburen, D. H. Madison, and N. Stolterfoht, ENergy and Angular Distribution of Electrons Ejected by Fast Protons and Electrons: Theory and Experiment, *Phys. Rev. A* 12: 60-79 (1975).

R. E. Mathis and D. A. Vroom, The Energy Distributions of Secondary Electrons from Ar, N_2, H_2O and H_2O with Clusters Present, *J. Chem. Phys.* 64: 1146-1149 (1976).

N. Oda, Energy and Angular Distributions of Electrons from Atoms and Molecules by Electron Impact, *Radiat. Res.* 64: 80-95 (1975).

N. Oda and F. Nishimura, Energy and Angular Distributions of Electrons Ejected from He and H_2 Bombarded by Equal Velocity H_2^+ and He^+ Ions, in XI International Conference on the Physics of Electronics and Atomic Collisions, Abstracts of Papers (The Society for Atomic Collision Research, Japan), pp. 622-623 (1979).

N. Oda, F. Nishimura, and S. Tahira, Energy and Angular Distributions of Secondary Electrons Resulting from Ionizing Collisions of Electrons with Helium and Krypton, *J. Phys. Soc. Japan* 33: 462-467 (1972).

C. B. Opal, E. C. Beaty, and W. K. Peterson, Tables of Energy and Angular Distributions of Electrons Ejected from Simple Gases by Electron Impact, Joint Institute for Laboratory Astrophysics (JILA) Report No. 108, University of Colorado, Boulder, CO (1971).

C. B. Opal, E. C. Beaty, and W. K. Peterson, Tables of Secondary Electron Production Cross Sections, *Atomic Data* 4: 209-253 (1972).

C. O. Reinhold, D. R. Schultz, R. E. Olson, L. H. Toburen, and R. D. DuBois, Electron Emission from Both Target and Projectile in C^+ + He Collisions, *J. Phys. B* 23: L297-L302 (1990).

M. E. Rudd, Energy and Angular Distributions of Secondary Electrons from 5-100 keV Proton Collisions with Hydrogen and Nitrogen Molecules, *Phys. Rev. A* 20: 787-796 (1979).

M. E. Rudd and R. D. DuBois, Absolute Doubly Differential Cross Sections for Ejection of Secondary Electrons from Gases by Electron Impact. I. 100 and 200 eV Electrons on Helium, *Phys. Rev. A* 16: 26-32 (1977).

M. E. Rudd and T. Jorgensen, Jr., Energy and Angular Distributions of Electrons Ejected from Hydrogen and Helium Gas by Protons, *Phys. Rev.* 131: 666-675 (1963).

M. E. Rudd, T. Jorgensen, Jr., and D. J. Volz, Electron Energy Spectrum from Ar^+ - Ar and H^+ - Ar Collisions, *Phys. Rev.* 151: 28-31 (1966).

M. E. Rudd and D. H. Madison, Comparison of Experimental and Theoretical Electron Ejection Cross Sections in Helium by Proton Impact from 5 to 100 keV, *Phys. Rev. A* 14: 128-136 (1976).

M. E. Rudd, J. S. Risley, J. Fryar, and R. G. Rolfes, Angular and Energy Distribution of Electrons form 15-to 150-keV H^0 + He Collisions, *Phys. Rev. A* 21: 506-514 (1980).

M. E. Rudd, C. A. Sautter, and C. L. Bailey, Energy and Angular Distributions of Electrons Ejected from Hydrogen and Helium by 100 to 300 keV Protons, *Phys. Rev.* 151: 20-27 (1966).

M. E. Rudd, L. H. Toburen, and N. Stolterfoht, Differential Cross Sections for Ejection of Electrons from Helium by Protons, *Atomic Data and Nuclear Data Tables* 18: 413-432 (1976).

M. E. Rudd, L. H. Toburen, and N. Stolterfoht, Differential Cross Sections for Ejection of Electrons from Argon by Protons, *Atomic Data and Nuclear Data Tables* 23: 405-442 (1979).

M. E. Rudd, G. L. Webster, C. A. Blocker, and C. A. Madison, Ejection of Electrons from Helium by Protons from 5-100 keV, in IX International Conference on the Physics of Electronic and Atomic Collisions, Abstracts of Papers (University of Washington Press, Seattle) pp. 745-746 (1975).

M. Sataka, K. Okuno, J. Urakawa, and N. Oda, Doubly Differential Cross Sections of Electron Ejection from Argon by 5-20 keV H^+, H_2^+, and He^+, in International Conference on the Physics of Electronic and Atomic Collisions, Abstracts of Papers (The Society of Atomic Collision Research, Japan) pp. 620-621 (1979).

M. Sataka, J. Urakawa, and N. Oda, Measurements of Double Differential Cross Sections for Electrons Ejected from 5-20 keV H^+, H_2^+, and He^+ Impacts on Argon, *J. Phys. B* 12: L729-L734 (1979).

S. Schmidt, J. Euler, C. Kelbch, S. Kelbch, R. Koch, G. Kraft, R. E. Olson, U. Ramm, J. Ullrich, and H. Schmidt-Böcking, Doubly Differential Stopping Powers of 1.4 MeV/amu U^{33+} in Ne and Ar Derived from Electron Production and Multiple Ionization Cross Sections, GSI-89-19, Gesellschaft fÜr Schwerionenforschung mbH, D-6100 Darmstadt, W. Germany (1989).

D. Schneider, D. DeWitt, A. S. Schlachter, R. E. Olson, W. G. Graham, J. R. Mowat, R. D. DuBois, D. H. Loyd, V. Nontemayor, and G. Schiwietz, Strong Continuum-Continuum Couplings in the Direct Ionization of Ar and He Atoms by 6-MeV/amu U^{38+} and Th^{38+} Projectiles, *Phys. Rev. A* 40: 2971-2975 (1989).

T. W. Shyn, Doubly Differential Cross Sections of Secondary Electrons Ejected from Gases by Electron Impact: 50-400 eV on N_2, *Phys. Rev. A* 27: 2388-2395 (1983).

T. W. Shyn and W. E. Sharp, Doubly Differential Cross Sections of Secondary Electrons Ejected from Gases by Electron Impact: 50-300 eV on Helium, *Phys. Rev. A* 19: 557-567 (1979a).

T. W. Shyn and W. E. Sharp, Doubly Differential Cross Sections of Secondary Electrons Ejected from Gases by Electron Impact: 50-400 eV on CO_2, *Phys. Rev. A* 20: 2332-2339 (1979b).

T. W. Shyn, W. E. Sharp, and Y. K. Kim, Doubly Differential Cross Sections of Secondary Electrons Ejected from Gases by Electron Impact: 25-250 eV on H_2, *Phys. Rev. A* 24: 79-88 (1981).

N. Stolterfoht, Angular and Energy Distributions of Electrons Produced by 200-500 keV Protons in Gases II. Results for Nitrogen, *Z. Physik* 248: 92-99 (1971a).

N. Stolterfoht, Energy and Angular Distribution of Electrons Ejected from Atoms Ionized by Protons, in VII International Conference on the Physics of Electronic and Atomic Collisions, Abstracts of Papers (North Holland, Amsterdam) pp. 1123-1125 (1971b).

N. Stolterfoht and D. Schneider, Double Differential Cross Sections for Electron Emission from Argon by 50- 500-keV N^+ and O^+ Impact, in Proceedings of the Fifth Conference on the Use of Small Accelerators, IEEE Transactions on Nuclear Science NS-26, 1130-1135 (1979).

N. Stolterfoht, D. Schneider, D. Burch, H. Wieman, and J. S. Risley, Mechanisms for Electron Production in 30-MeV O^{n+} + O_2 Collisions, *Phys. Rev. Lett.* 33: 59-62 (1974).

N. Stolterfoht, D. Schneider, J. Tanis, H. Altevogt, A. Salin, P. D. Fainstein, R. Rivarola, J. P. Grandin, J. N. Scheurer, S. Andriamonje, D. Bertault, and J. F. Chemin, Evidence for Two-Center Effects in the Electron Emission from 25 MeV/amu Mo^{40+} + He Collisions: Theory and Experiment, *Europhysics Lett.* 4: 899-904 (1987).

L. H. Toburen, Distributions in Energy and Angle of Electrons Ejected from Molecular Nitrogen by 0.3-1.7 MeV Protons, *Phys. Rev. A* 3: 216-228 (1971a).

L. H. Toburen, Angular Distributions of Electrons Ejected by Fast Protons, Vii International Conference on the Physics of Electronic and Atomic Collisions, Abstracts of Papers (North Holland, Amsterdam) pp. 1120-1122 (1971).

L. H. Toburen, Distributions in Energy and Angle of Electrons Ejected from Xenon by 0.3 to 2.0 MeV Protons, *Phys. Rev. A* 9: 2505-2517 (1974).

L. H. Toburen, Secondary Electron Emission in Collisions of 1.2 MeV C^+ Ions with He, Ne, Ar, and CH_4, in XI International Conference on the Physics of Electronic and Atomic Collisions, Abstracts of Papers (The Society for Atomic Collisions Research, Japan) pp. 630-631 (1979).

L. H. Toburen, Differential Cross Sections for Electron Emission in Heavy Ion-Atom Collisions, in Proceedings of the Fifth Conference on the use of Small Accelerators, IEEE Transactions on Nuclear Science NS-26, 1056-1061 (1979b).

L. H. Toburen and S. T. Manson, On the Unreliability of the Hydrogenic Approximation for Inelastic Collision of Fast Charged Particles with Atoms: Ionization of Neon by Protons, in VIII International Conference on the Physics of Electronic and Atomic Collisions, Abstracts of Papers (Institute of Physics, Belgrad) pp. 695-696 (1973).

L. H. Toburen and S. T. Manson, Differential Cross Sections for Ionization of Krypton by Fast Protons. Theory and Experiment, in XI International Conference on the Physics of Electronic and Atomic Collisions, Abstracts of Papers (The Society for Atomic Collision Research, Japan) pp. 628-629 (1979).

L. H. Toburen, S. T. Manson, and Y.-K. Kim, Energy Distributions of Secondary Electrons. III: Projectile Energy Dependence for Ionization of He, Ne, and Argon by Protons, *Phys. Rev. A* 17: 148-159 (1978).

L. H. Toburen, and W. E. Wilson, Distributions in Energy and Angle by Electrons Ejected from Molecular Hydrogen by 0.3-1.5 MeV Protons, *Phys. Rev. A* 5: 247-256 (1972).

L. H. Toburen and W. E. Wilson, Energy and Angular Distributions of Electrons Ejected from Water Vapor by 0.3 - 1.5 MeV Protons, *J. Chem. Phys.* 66: 5202-5213 (1977a).

L. H. Toburen and W. E. Wilson, Ionization of Noble Gases by Equal Velocity He^{+}, He^{++}, and H^{+} Ions, in X International Conference on the Physics of Electronic and Atomic Collisions, Abstracts of Papers (Commissariat A L'Energie Atomique, Paris) pp. 1006-1007 (1977).

L. H. Toburen and W. E. Wilson, Differential Cross Sections for Ionization of Argon by .3-2 MeV He^{2+} and He^{+} Ions, *Phys. Rev. A* 19: 2214-2224 (1979).

L. H. Toburen, W. E. Wilson, and R. J. Popowich, Secondary Electron Emission from Ionization of Water Vapor by 0.3- to 2.0-MeV He^{+} and He^{2+} Ions, *Radiat. Res.* 82: 27-44 (1980).

L. H. Toburen, W. E. Wilson, and L. E. Porter, Energy and Angular Distributions of Electrons Ejected in Ionization of SF_6 and TeF_6 by Fast Protons, *J. Chem. Phys.* 4212-4221 (1977).

J. Urakawa, N. Tokoro, and N. Oda, Differential Cross Sections for Ejection of Electrons and Dissociative Ionization Cross Sections for 5-20 keV H_2^{+} and H_3^{+} Impacts on Helium, *J. Phys. B* 14: L431-L435 (1981).

W. E. Wilson and L. H. Toburen, Electron Emission in H_2^{+} - H_2 Collisions from 0.6 to 1.5 MeV, *Phys. Rev. A* 7: 1535-1544 (1973).

W. E. Wilson and L. H. Toburen, Electron Emission from Proton-Hydrocarbons-Molecule Collisions at 0.3 to 2 MeV, *Phys. Rev. A* 11: 1303-1308 (1975).

P. H. Woerlee, Yu. S. Gordeev, H. de Waard, and F. W. Saris, The Production of Continuous Electron Spectra in Collisions of Heavy Ions and Atoms. B: Direct Coupling with the Continuum, *J. Phys. B* 14: 527-539 (1981).

END

DATE FILMED

12/28/90